Cell Reports

Resource

A human adipose tissue cell-type transcriptome atlas

Graphical abstract

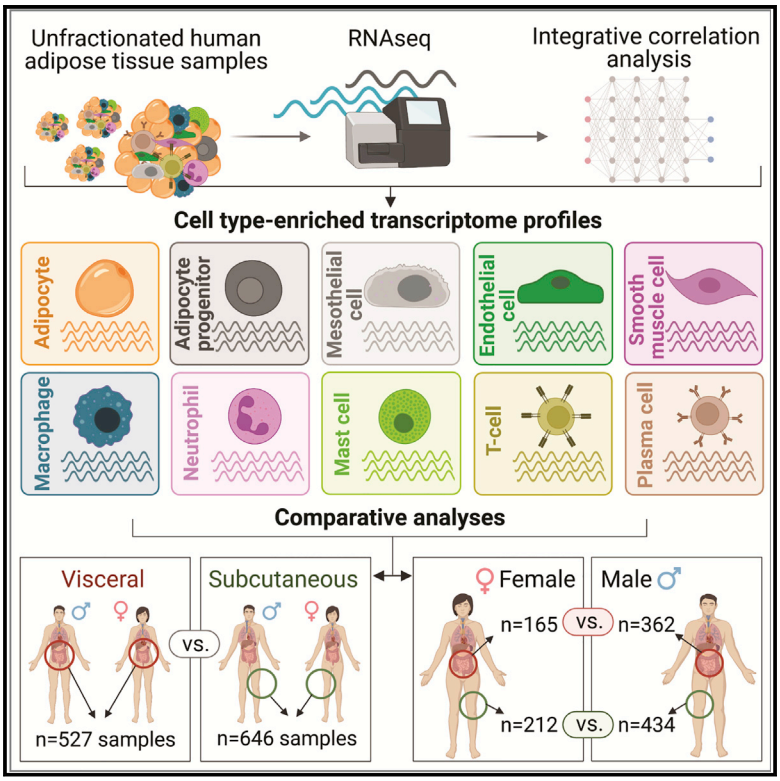

Authors

Marthe Norreen-Thorsen, Eike Christopher Struck, Sofia Öling, ..., Mathias Uhlén, Philip James Dusart, Lynn Marie Butler

Correspondence

lynn.butler@ki.se, lynn.m.butler@uit.no

In brief

Norreen-Thorsen et al. use an integrative correlation analysis of human adipose tissue RNA-seq data, identifying >2,000 cell-type-enriched coding and non-coding transcripts. Comparative analyses highlight transcripts with visceral and subcutaneous depot-specific and/or sex-specific cell-type enrichment. The method allows profiling of adipocytes, whose physical characteristics make analysis with other methods challenging.

Highlights

- Uses publicly available adipose tissue bulk RNA-seq data from two human fat depots
- Enriched genes in 10 cell types profiled using an integrative correlation analysis
- Comparative analysis identifies depot- and sex-specific cell-type-enriched genes
- Method circumvents technical challenges with adipose tissue scRNA-seq analysis

Norreen-Thorsen et al., 2022, Cell Reports *40*, 111046
July 12, 2022
https://doi.org/10.1016/j.celrep.2022.111046

CellPress

Cell Reports

CellPress
OPEN ACCESS

Resource

A human adipose tissue cell-type transcriptome atlas

Marthe Norreen-Thorsen,[1] Eike Christopher Struck,[1] Sofia Öling,[1] Martin Zwahlen,[2] Kalle Von Feilitzen,[2] Jacob Odeberg,[1,2,3,4] Cecilia Lindskog,[5] Fredrik Pontén,[5] Mathias Uhlén,[2] Philip James Dusart,[1,2,6,7] and Lynn Marie Butler[1,2,6,7,8,*]

[1]Translational Vascular Research, Department of Clinical Medicine, The Arctic University of Norway, 9019 Tromsø, Norway
[2]Science for Life Laboratory, Department of Protein Science, Royal Institute of Technology (KTH), 171 21 Stockholm, Sweden
[3]The University Hospital of North Norway (UNN), 9019 Tromsø, Norway
[4]Coagulation Unit, Department of Hematology, Karolinska University Hospital, 171 76 Stockholm, Sweden
[5]Department of Immunology, Genetics and Pathology, Science for Life Laboratory, Uppsala University, 752 37 Uppsala, Sweden
[6]Clinical Chemistry and Blood Coagulation Research, Department of Molecular Medicine and Surgery, Karolinska Institute, 171 76 Stockholm, Sweden
[7]Clinical Chemistry, Karolinska University Laboratory, Karolinska University Hospital, 171 76 Stockholm, Sweden
[8]Lead contact
*Correspondence: lynn.butler@ki.se or lynn.m.butler@uit.no
https://doi.org/10.1016/j.celrep.2022.111046

SUMMARY

The importance of defining cell-type-specific genes is well acknowledged. Technological advances facilitate high-resolution sequencing of single cells, but practical challenges remain. Adipose tissue is composed primarily of adipocytes, large buoyant cells requiring extensive, artefact-generating processing for separation and analysis. Thus, adipocyte data are frequently absent from single-cell RNA sequencing (scRNA-seq) datasets, despite being the primary functional cell type. Here, we decipher cell-type-enriched transcriptomes from unfractionated human adipose tissue RNA-seq data. We profile all major constituent cell types, using 527 visceral adipose tissue (VAT) or 646 subcutaneous adipose tissue (SAT) samples, identifying over 2,300 cell-type-enriched transcripts. Sex-subset analysis uncovers a panel of male-only cell-type-enriched genes. By resolving expression profiles of genes differentially expressed between SAT and VAT, we identify mesothelial cells as the primary driver of this variation. This study provides an accessible method to profile cell-type-enriched transcriptomes using bulk RNA-seq, generating a roadmap for adipose tissue biology.

INTRODUCTION

Adipose tissue acts as an energy depot, provides insulation, and is an important endocrine organ that communicates with other tissues to regulate systemic metabolism (Kahn et al., 2019). Most adipose tissue in adults is white adipose tissue, broadly categorized as visceral adipose tissue (VAT), located deep in the abdomen and around internal organs, or subcutaneous adipose tissue (SAT), located under the skin. Excess VAT is associated with metabolic disorders, e.g., diabetes and cardiovascular disease (Britton et al., 2013; Chait and den Hartigh, 2020; Oikonomou and Antoniades, 2019), while SAT is associated with reduced risk, possibly even protection (Lumish et al., 2020). Recent studies have profiled differences in gene expression between adipose depots using bulk RNA sequencing (RNA-seq) (Bradford et al., 2019; Schleinitz et al., 2020), but the relative contribution of specific cell types to the observed differences is not known.

Adipose tissue contains adipocytes, adipocyte progenitor cells, endothelial cells, smooth muscle cells, stromal cells, and immune cell types, including macrophages and T cells (Lu et al., 2019). Single-cell RNA-seq (scRNA-seq) has been used to profile macrophages, endothelial cells, fibroblasts, and adipocyte progenitors from human VAT or SAT (Acosta et al., 2017; Esteve et al., 2019; Vijay et al., 2020). Such studies provide high resolution of different cell (sub)types but are limited by the requirement for fresh tissue, low number of biological replicates, and compromised read depth (Beliakova-Bethell et al., 2014; Rizzetto et al., 2017; Saliba et al., 2014; Ziegenhain et al., 2017). Furthermore, the analysis of adipocytes, the major functional cell type in adipose tissue, is challenging; with high buoyancy and large size, they require extensive, artefact-generating proteolytic digestion for tissue separation (Rondini and Granneman, 2020; Viswanadha and Londos, 2006), and thus, adipocyte data are absent from many scRNA-seq datasets (e.g., Hildreth et al., 2021; Karlsson et al., 2021; Tabula Muris et al., 2018; Tabula Sapiens et al., 2022; Vijay et al., 2020). Progenitor cells isolated from human adipose tissue have been used to generate adipocytes in culture for analysis (Min et al., 2019), but potential phenotype modifications, due to induced differentiation in the absence of the native microenvironment, are a limitation of this model. Transgenic labeling of cell-type-specific

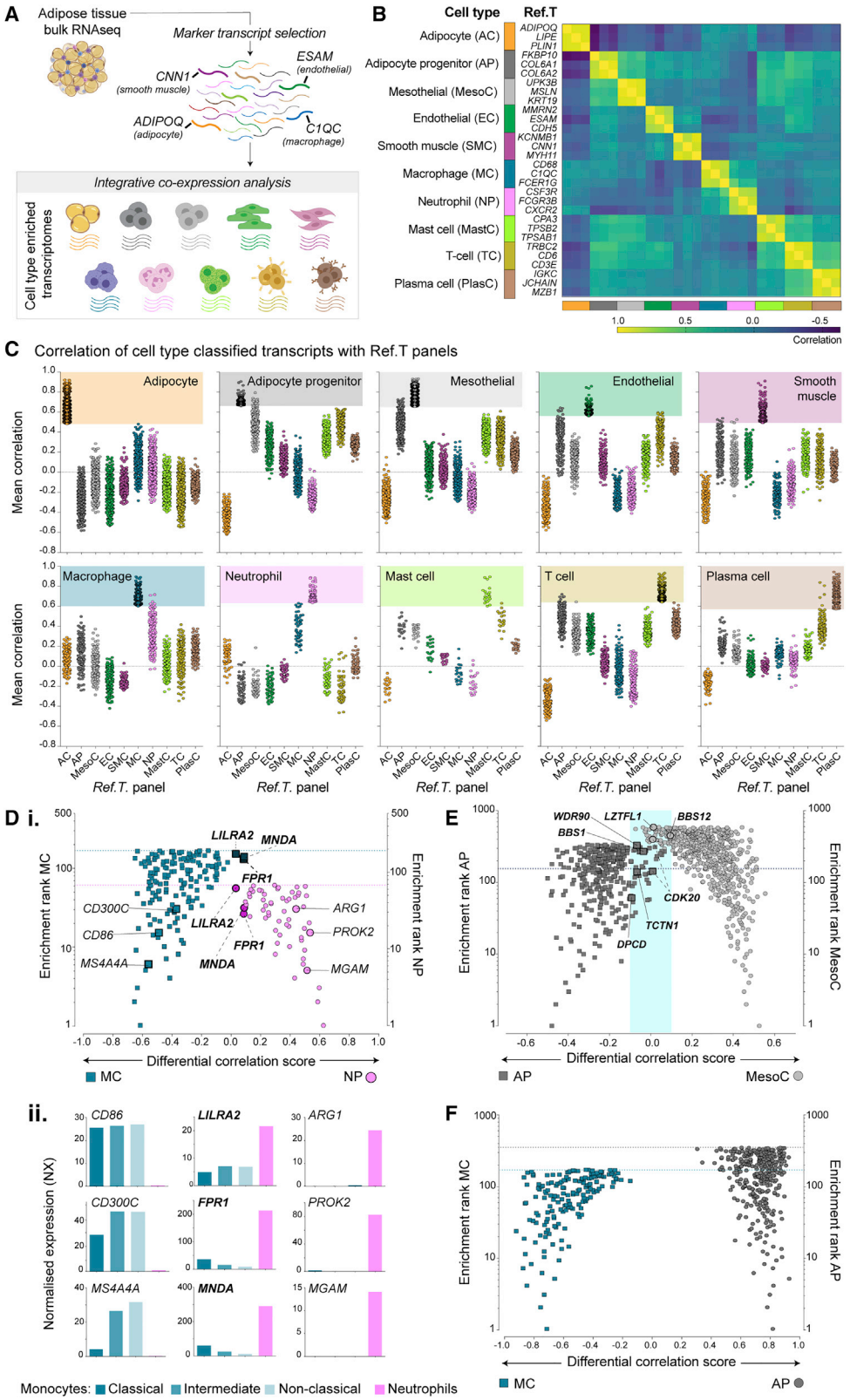

(legend on next page)

mRNA (Roh et al., 2017) has been used to overcome these technical problems for analysis of murine adipocytes, but this cannot be applied to human tissue. Adipocytes have been analyzed using single-nuclei RNA-seq, circumventing some scRNA-seq limitations, but transcript expression can differ between nuclei and cytoplasm (Thrupp et al., 2020). Non-coding RNA is emerging as a novel, important class of molecules in adipose biology (Squillaro et al., 2020; Xu and Sun, 2020), but to date, there is no description of adipose-cell-type-specific non-coding RNAs.

Here, using an analysis approach to circumvent technical challenges associated with profiling individual cell types in adipose tissue, we identified over 2,300 transcripts with cell-type-enriched expression. Of all cell types profiled, adipocytes had the highest number of enriched transcripts and the greatest proportion of non-coding. Comparisons between female and male samples revealed a panel of cell-type-enriched Y-linked transcripts, of which three were adipocyte enriched in both depots. Finally, we resolve the overall differences in gene expression between VAT and SAT to a cell-type level, uncovering the primary driver to be cell-type composition, specifically the presence of mesothelial cells in VAT, but not SAT. Data are available through the Human Protein Atlas portal (www.proteinatlas.org/humanproteome/tissue+cell+type/adipose+tissue).

RESULTS

Identification of cell-type transcriptome profiles in visceral adipose tissue

Cell-type reference transcripts correlate across unfractionated adipose RNA-seq data

VAT is linked to the development of metabolic dysfunction and associated disorders (Chait and den Hartigh, 2020). To identify cell-type-enriched transcriptome profiles, we performed an analysis based on our previously reported method (Butler et al., 2016; Dusart et al., 2019) (concept summary, Figures 1A and S1A), using VAT RNA-seq data (n = 527) from Genotype-Tissue Expression (GTEx) portal v.8 (www.gtexportal.org) (Consortium, 2015). For each cell type, a panel of three marker genes were selected (“reference transcripts” [*Ref.T.*s]). Correlation coefficients (corr.) between the expression levels of the *Ref.T.*s and all other sequenced transcripts were calculated across samples; those that highly and selectively correlated with the *Ref.T.* panel were classified as enriched in the corresponding cell type (Figure S1A). We shortlisted candidate *Ref.T.*s for all main constituent cell types, including (1) well-established markers identified in older “none-omics” studies (e.g., Hu et al., 1996); (2) markers identified by scRNA-seq of mouse (Tabula Muris et al., 2018) or human (Han et al., 2020) adipose tissue; (3) marker lists from large databases containing data from multiple sources, e.g., Cell Marker (Zhang et al., 2019) and PanglaoDB (Franzen et al., 2019); and (4) commercial marker panels (e.g., https://www.rndsystems.com/). VAT RNA-seq data were processed to generate Spearman correlation coefficients (corr.s) between all candidate *Ref.T.*s and a panel selected to represent each cell type, based on the following criteria: (1) a high corr. (minimum 0.70) between *Ref.T.*s within each cell type panel (Figure 1B; Table S1, tab 1, table A), consistent with cell type co-expression; adipocyte panel (*ADIPOQ*, *LIPE*, and *PLIN1*; mean corr. ± SD 0.91 ± 0.002), adipocyte progenitor panel (*FKBP10*, *COL6A1*, and *COL6A2*; 0.86 ± 0.06), mesothelial panel (*UPK3B*, *MSLN*, and *KRT19*; 0.92 ± 0.02), endothelial panel (*MMRN2*, *ESAM*, and *CDH5*; 0.80 ± 0.03), smooth muscle panel (*KCNMB1*, *CNN1*, and *MYH11*; 0.80 ± 0.06), macrophage panel (*CD68*, *C1QC*, and *FCER1G*; 0.83 ± 0.03), neutrophil panel (*CSF3R*, *FCGR3B*, and *CXCR2*; 0.81 ± 0.04), mast cell panel (*CPA3*, *TPSB2*, and *TPSAB1*; 0.83 ± 0.03), T cell panel (*TRBC2*, *CD6*, and *CD3E*; 0.89 ± 0.02), and plasma cell panel (*IGKC*, *JCHAIN*, and *MZB1*; 0.89 ± 0.04; all $p < 4.0 \times 10^{-99}$); (2) a low corr. between *Ref.T.*s in different cell type panels (Figure 1B; Table S1, tab 1, table A), consistent with high specificity of each panel (mean inter-panel corr. ± SD 0.05 ± 0.25); and (3) a normal distribution of *Ref.T.* expression across samples (Figure S1B). Candidate B cell *Ref.T.*s were lowly expressed in VAT, with low intra-panel corr. (Table S1, tab 2, table A). In a comparative dataset, human spleen RNA-seq, GTEx v.8 (n = 241), selected due to high B cell content, the candidate B cell *Ref.T.*s were highly expressed and strongly correlated with each other (Table S1, tab 2, table B). Thus, B cells were excluded from subsequent profiling of VAT, due to presumed low numbers or absence from a large proportion of VAT samples. Candidates within the panels selected as potential *Ref.T.*s for pericytes, lymphatic endothelial cells, and dendritic cells did not correlate as well as those selected to represent other cell types (Table S1, tab 2, tables C, D, and E, respectively), consistent with previous reports that these cell types lack multiple highly

Figure 1. Integrative co-expression analysis of unfractionated human visceral adipose tissue (VAT) RNA-seq can resolve constituent cell-type identities

(A) Overview of analysis concept; human VAT RNA-seq data (n = 527 individuals) were retrieved from GTEx portal v.8 and constituent cells “virtually tagged” using cell-type-specific reference transcripts (*Ref.T.*s). Integrative co-expression analysis was used to identify transcripts with comparable profiles.

(B) Heatmap of Spearman correlation (corr.) values between *Ref.T.* panels selected for VAT cell types: adipocyte (AC), adipocyte progenitor (AP), mesothelial (MesoC), endothelial (EC), smooth muscle (SMC), macrophage (MC), neutrophil (NP), mast cell (MastC), T cell (TC), and plasma cell (PlasC).

(C) Mean corr. values between genes above designated threshold (see results section for criteria) and all *Ref.T.* panels.

(D) (i) For transcripts above the designated corr. threshold with macrophage (squares, MC) or neutrophil (circles, NP) *Ref.T.* panels, the “differential corr. score” (difference between mean corr. with MC and NP *Ref.T.*s) was plotted versus “enrichment ranking” (position in each respective list; highest corr. = rank 1). Corresponding colored lines indicate numbers above the designated threshold. Bold text annotations show transcripts in *both* MC and NP lists (circular *and* square symbol on the same x axis dimension). (ii) scRNA-seq data from the Human Protein Blood Atlas (Uhlen et al., 2019) showing gene expression in classical, intermediate, and non-classical monocytes and neutrophils from whole blood.

(E and F) Comparative plots for transcripts are classified as (E) adipocyte progenitor (AP) or mesothelial (MesoC) enriched (shaded blue box indicates co-enriched genes) and (F) MC or AP enriched.

See also Figures S1 and S2 and Tables S1, tabs 1, 4a, and 4b, and S2, tab 1.

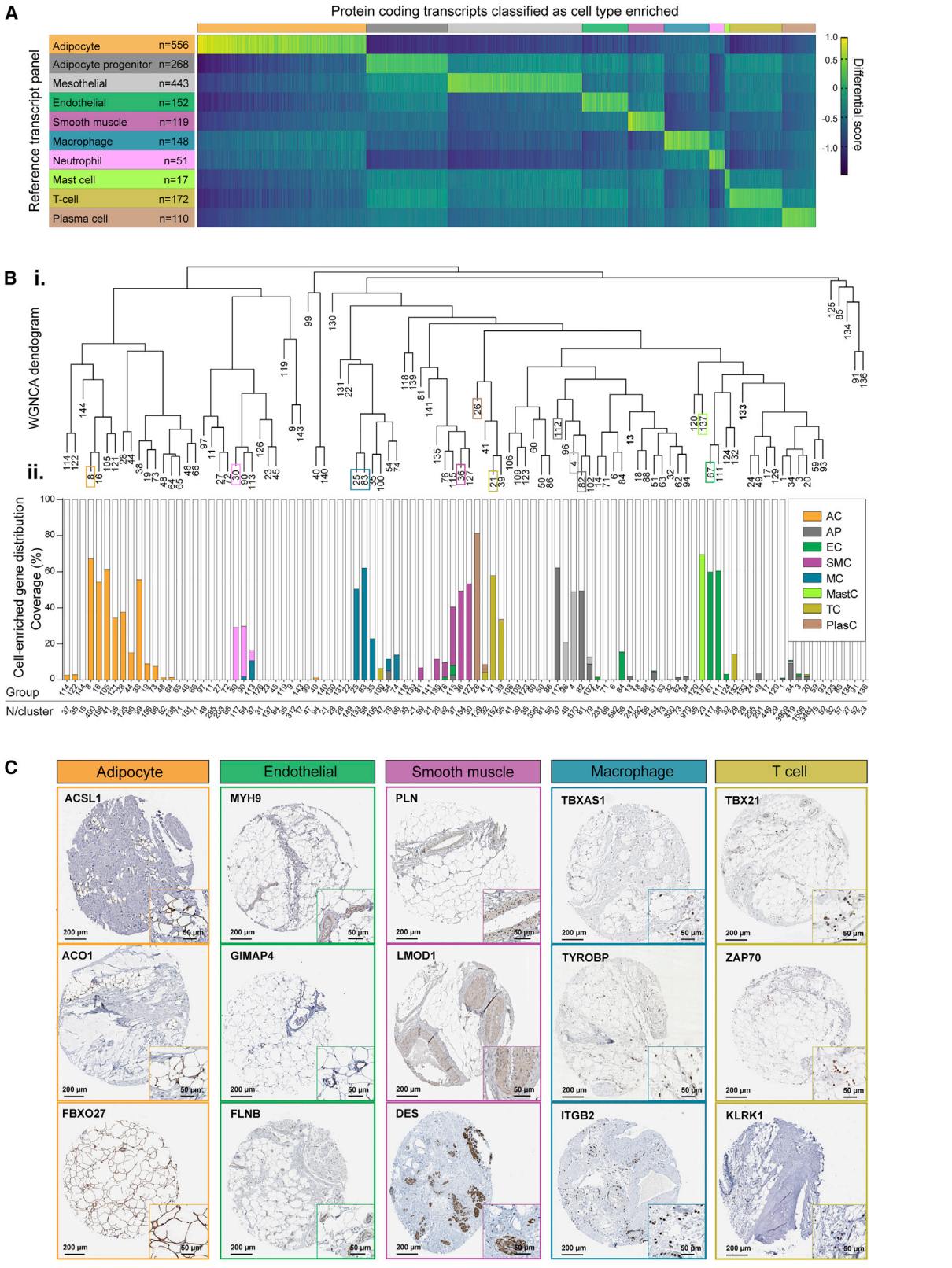

(legend on next page)

specific pan-markers (Armulik et al., 2011; Sichien et al., 2017; Takeda et al., 2019). Thus, they were not included in the subsequent analysis.

Reference transcripts analysis can identify distinct cell-type-associated transcripts

We generated corr.s between each *Ref.T.* and all sequenced transcripts (~53,625) across VAT samples. The proportion of constituent cell types between samples vary, due to both sampling and heritability factors (Glastonbury et al., 2019), but ratios between cell-specific co-expressed genes should remain constant. Thus, a high corr. of a given transcript with all *Ref.T.*s in any one panel is consistent with expression in the corresponding cell type. For each *Ref.T.* panel, a list of such transcripts was generated using a corr. value threshold cutoff, which was either (1) that above which >95% of transcripts reached this threshold with *only* that *Ref.T.* panel or (2) $\geq$0.50, whichever was higher (for thresholds, see Table S1, Tab 1, Table B). Resultant transcripts were generally well separated (Figure 1C), but some overlap was observed between closely related cell types, e.g., macrophages [MCs] and neutrophils [NPs]; Figure 1C, row 2). To compare specific transcripts in two cell-type classified groups, e.g., MC and NP enriched (Figure 1D.i), the following was calculated for each transcript: (1) the "differential correlation score," defined as the difference between the mean corr. with the two sets of *Ref.T.*s, i.e., MC panel (*CD68*, *C1QC*, and *FCER1G*) and NP panel (*CSF3R*, *FCGR3B*, and *CXCR2*), and (2) the "enrichment ranking," based on the mean corr. value with the *Ref.T.* panel (rank 1 = highest corr.). Three transcripts were provisionally classified as both MC and NP enriched: *LILRA2*, *MNDA*, and *FPR1* (Figure 1D.i; gene IDs in bold text). *LILRA2* had comparable corr. with both MC and NP *Ref.T.* panels (mean corr. ± SD: 0.61 ± 0.07 and 0.65 ± 0.07, respectively), while *MNDA* and FPR1, despite reaching the threshold for both, were more highly correlated with the NP *Ref.T.* panel than the MC panel (*MNDA*: NP 0.71 ± 0.04 versus MC 0.62 ± 0.08 and *FPR1*: NP 0.72 ± 0.07 versus MC 0.63 ± 0.14). We extracted expression data for these genes in monocytes (MonoC) and neutrophils in blood (Figure 1D.ii) from scRNA-seq generated as part of our Human Protein Atlas (HPA) blood atlas (Uhlen et al., 2019). In all three cases, these transcripts were expressed in both MonoC and NP (Figure 1D.ii, central column). In contrast, transcripts we classified as enriched *only* in MC (*CD300C*, *CD86*, and *MS4A4A*) or *only* in NP (*ARG1*, *PROK2*, and *MGAM*) were predominantly expressed in MonoC or NP in blood, respectively (Figure 1D.ii). Although MonoC and MC are not directly comparable, the majority of the monocyte transcriptional profile is maintained during differentiation (Martinez et al., 2006), and so these data support our annotated classifications. These annotations were also consistent with data from scRNA-seq of macrophages and neutrophils from human SAT (Tabula Sapiens et al., 2022; Figure S2B). Thus, to exclude potentially dual-enriched transcripts from cell-type classification, we excluded transcripts with a differential corr. value < 0.1 versus any other *Ref.T.* panel. The highest number of transcripts excluded for this reason were those that correlated with both adipocyte progenitor cell and mesothelial cell *Ref.T.* panels; 84 transcripts were excluded from cell-type classification due to likely co-expression (Figure 1E; Table S1, tab 4a). Gene ontology (GO) and reactome analysis of this gene list revealed over-representation of terms related to "plasma membrane bounded cell projection organization" (false discovery rate [FDR] 1.26×10^{-2}) and "BBSome-mediated cargo targeting to cilium" (FDR 8.09×10^{-3}), respectively (Table S1, tab 4b, with selected examples highlighted in Figure 1E), suggesting a possible link to the importance of primary cilia in the regulation of adipose tissue expansion (Hilgendorf, 2021; Ritter et al., 2018). In most other cases, transcripts were well separated between cell types, e.g., MC classified versus adipocyte progenitor (AP) classified (Figure 1F). We classified 2,343 transcripts as cell-type enriched in VAT (Tables S1, tab 1, table B, and S2, tab 1), the majority of which (2,036 [87%]) were protein coding (Figure 2A).

Independent methods and datasets support cell-type classifications

Unsupervised weighted network correlation analysis (WGNCA) is consistent with Ref.T. analysis

As our analysis method is based on manually selected *Ref.T.* panels, cell-type classification is subject to an input bias. As a comparison, we analyzed the same dataset using an unbiased WGCNA (Langfelder and Horvath, 2008). Corr.s between all transcripts were calculated, and they were subsequently clustered into related groups, based on expression similarity (Figure 2B.i). Members of the same *Ref.T.* panels clustered into the same WGCNA group, e.g., adipocyte *Ref.T.*s (*ADIPOQ*, *LIPE*, and *PLIN1*; cluster 8, orange box) and mesothelial *Ref.T.*s (*UPK3B*, *MSLN*, and *KRT19*; cluster 4, light gray box, Figure 2B.i), or into adjacent leaves on the same clade, e.g., macrophage *Ref.T.*s (*CD68*, *C1QC*, and *FCER1G*; group 25 and 83, blue box, Figure 2B.i). The locations of all other *Ref.T.*s are indicated by the respective colored boxes. Thus, WGCNA results were consistent with intra-panel *Ref.T.*s having shared expression profiles (i.e., in a common cell type). Protein-coding transcripts classified as cell-type enriched (Figure 2A) predominantly clustered into the same WGCNA group(s) as the corresponding

Figure 2. Integrative co-expression analysis of unfractionated RNA-seq reveals enriched protein-coding transcriptomes of human visceral adipose tissue (VAT) cell types

(A) Heatmap of protein-coding transcripts classified as cell type enriched (indicated by horizontal colored bars), showing differential score between mean corr. with the corresponding *Ref.T.* panel versus highest mean corr. coefficient among the other *Ref.T.* panels.

(B) Human VAT RNA-seq data (n = 527 individuals) were subject to weighted correlation network analysis (WGCNA). (i) Colored squares indicate *Ref.T.* location on dendrogram (colors correspond to cell types as annotated in A). (ii) Distribution of protein-coding transcripts classified as cell type enriched across dendrogram groups.

(C) Human adipose tissue sections were stained using antibodies targeting proteins encoded by transcripts classified as adipocyte, endothelial, smooth muscle, macrophage, or T cell enriched. Scale bar, 200 μm; inset, 50 μm.

See also Table S2, tab 1, and Figure S3.

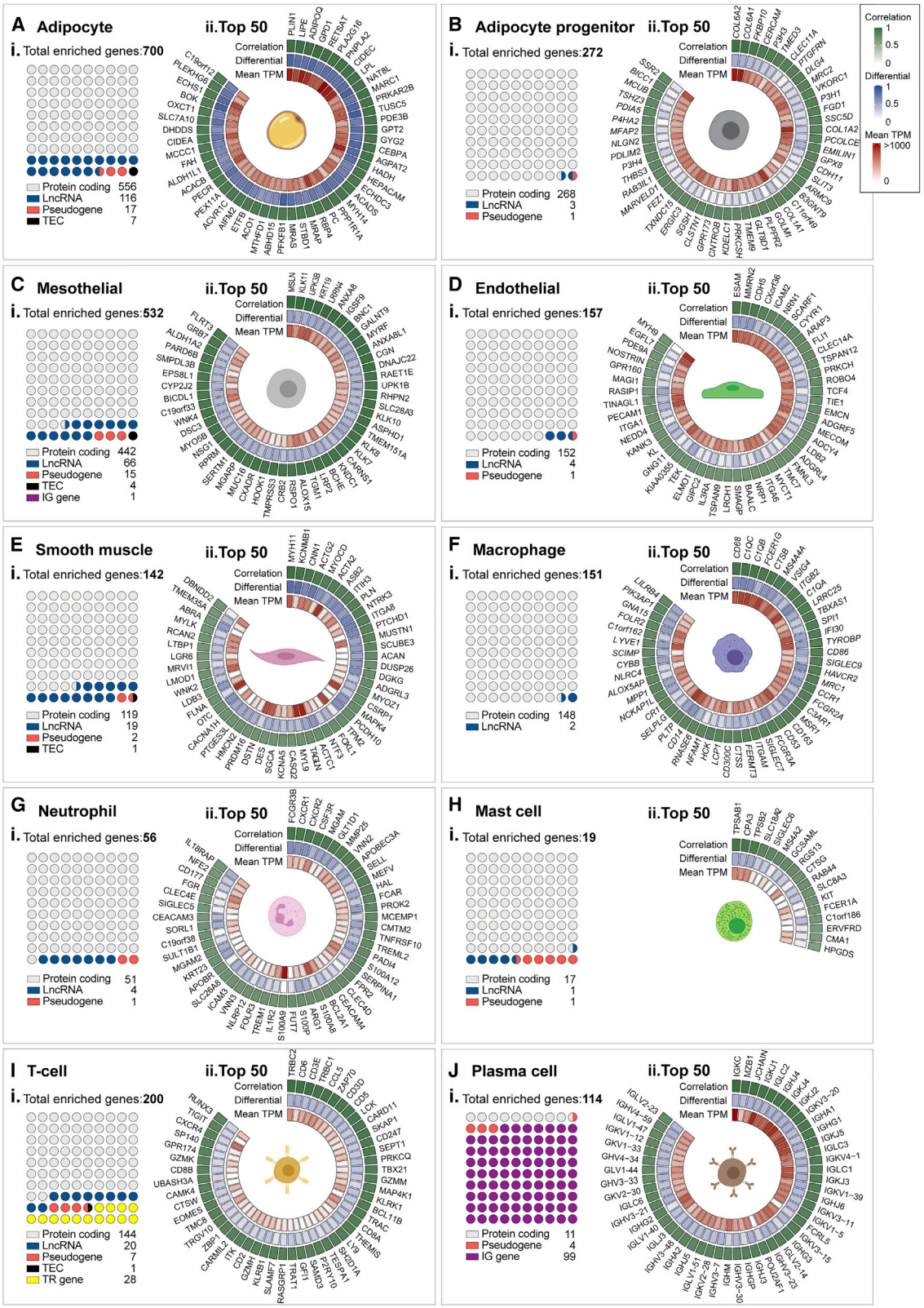

(legend on next page)

Ref.T.s, e.g., mast cell enriched (lime green bar, group 137) and macrophage enriched (blue bars, groups 25 and 83;, (Figure 2B.ii) and, in some cases, different leaves on a common clade, e.g., adipocyte enriched (orange bars, groups 8, 16, 105, 121, 28, 44, and 38) and smooth muscle cells (purple bars, groups 36, 127, and 115) Figure 2B.ii). Thus, protein-coding transcripts classified as cell-type enriched also clustered together in an unbiased WGCNA, consistent with cell type co-expression. Protein profiling of human adipose tissue is provided for selected adipocyte-, endothelial-, smooth-muscle-cell-, macrophage- and T-cell-enriched transcripts (Figures 2C and S3A).

Cell-type-enriched transcripts in visceral adipose tissue

Adipocytes had the most enriched transcripts (n = 700), of which the greatest proportion were protein coding (Figure 3A.i, light gray circles), followed by long non-coding RNA (lncRNA) and pseudogenes (Figure 3A.i; Vertebrate Genome Annotation [VEGA] database; Harrow et al., 2014). Mesothelial cells (Figure 3C.i), and adipocyte progenitor cells (Figure 3B.i) also had a relatively high number of enriched transcripts (n = 532 and 272, respectively), while immune cells, and other non-tissue-specific cells, had fewer: endothelial (n = 157) (Figure 3D.i), smooth muscle (n = 142) (Figure 3E.i), macrophages (n = 151) (Figure 3F.i), neutrophils (n = 56) (Figure 3G.i), mast cells (n = 19) (Figure 3H.i), T cells (n = 200) (Figure 3I.i), and plasma cells (n = 114) (Figure 3J.i; Table S2, tab 1). In most cell types, lncRNAs represented the majority of transcripts outside those classified as protein coding (Figures 3A.i–3J.i), with the notable exception of T cells and plasma cells, where the majority were T cell receptor (TR) (Figure 3I.i) or immunoglobulin (IG) genes (Figure 3J.i), respectively. GO and reactome analysis (Ashburner et al., 2000; Gene Ontology, 2021) was performed to identify over-represented classes and pathways in each list of enriched transcripts (Table S2, tabs 2–11). Results were consistent with known cell functions. For example, for adipocyte-enriched transcripts, most significant GO terms included "small molecule metabolic process" (FDR 2.5×10^{-60}) and "carboxylic acid metabolic process" (FDR 1.4×10^{-57}) and reactome pathways included "metabolism" (FDR 2.9×10^{-70}); for smooth muscle-enriched transcripts, GO terms included "muscle system processes" (FDR 5.9×10^{-14}) and reactome pathways included "muscle contraction" (FDR 1.9×10^{-9}); for endothelial-cell-enriched transcripts, GO terms included "blood vessel development" (FDR 8.8×10^{-10}) and "angiogenesis" (FDR 1.1×10^{-9}); and for neutrophil-enriched transcripts, GO terms included "neutrophil activation" (FDR 1.9×10^{-18}) and reactome pathways included "neutrophil degranulation" (FDR 5.6×10^{-19}) (for all cell types, see Table S2, tabs 2–11, tables Ai and Aii). We visualized the top 50 enriched protein-coding transcripts for each cell type (Figures 3A.ii–3J.ii), ranked by highest mean corr. with the *Ref.T*. panel, to compare differential corr. values (corr. with corresponding cell type *Ref.T*. panel minus max corr. with any other *Ref.T*. panel) and expression. Overall, expression values for enriched genes were highest for adipocytes (Figure 3A.ii), adipocyte progenitor cells (Figure 3B.ii), endothelial cells (Figure 3D.ii), macrophages (Figure 3F.ii), and plasma cells (Figure 3J.ii) and lowest for neutrophils, mast cells, and T cells (Figures 3G.ii–3I.ii). However, cell-type-enriched transcripts had a range of expression values, indicating variation in regulatory mechanisms, transcript stability, or presence of cell subtypes.

Cell-type-enriched non-coding transcripts in VAT

We classified 307 non-coding transcripts as cell-type enriched in VAT, the highest number of which were in adipocytes (n = 144), followed by mesothelial cells (n = 89) (Figure 4A; Table S2, tab 1). Cell-enriched non-coding transcripts were typically expressed at lower levels than cell-enriched protein-coding transcripts (mean transcripts per million [TPM] ± SD, protein coding: 45.4 ± 118.5 versus non-coding: 3.06 ± 5.2), with a higher frequency of samples with low or no expression (mean % samples with expression >0.1 TPM ± SD, coding 2.7 ± 7.8 versus non-coding 12.4 ± 14.9). Cell-type-enriched non-coding transcripts predominantly clustered into the same WGCNA group(s)/clades as the corresponding protein-coding *Ref.T*.s (Figures 4A.ii and 4A.iii, *Ref T*. location marked by colored boxes), e.g., adipocyte enriched (orange ovals, groups 8, 16, 105, 121, 28, 44, and 38; Figure 4A.iii), consistent with cell type co-expression. We visualized up to the top 50 enriched non-coding transcripts for the four cell types with the highest number (Figures 4B.i–4B.iv), ranked by highest mean corr. with the *Ref.T*. panel, to compare differential corr. values (corr. with corresponding cell type *Ref.T*. panel minus max corr. with any other *Ref.T*. panel) and expression. Overall, expression values for non-coding enriched genes were highest for adipocytes (Figure 4B.i). Although there is no comparable existing dataset to validate these results, we used scRNA-seq data from the analysis of human SAT (Tabula Sapiens et al., 2022; Figure 4C.i) to make some comparisons. Although this dataset does not include adipocytes or mesothelial cells (those with the highest number of predicted enriched non-coding transcripts) and lacks data for many non-coding transcripts, it provides supportive evidence for our classifications in the other cell types (Figures 4C.ii–4C.viii). All enrichment scores for non-coding transcripts can be searched via the web portal https://cell-enrichment.shinyapps.io/noncoding/.

Identification of cell-type transcriptome profiles in subcutaneous adipose tissue (SAT)

White adipose tissue is broadly classified by location; VAT is intra-abdominal, adjacent to internal organs, while SAT lies underneath the skin. The proportion of VAT to SAT increases in obesity and is linked to metabolic dysregulation (Chait and den Hartigh, 2020). In order to compare these two depots, SAT-cell-type-enriched profiles were determined as described for VAT, using human SAT RNA-seq data (n = 646) from GTEx portal

Figure 3. Core transcriptional identities of human VAT cell types

Cell-type-enriched transcripts in (A) adipocytes, (B) adipocyte progenitor cells, (C) mesothelial cells, (D) endothelial cells, (E) smooth muscle cells, (F) macrophages, (G) neutrophils, (H) mast cells, (I) T cells, and (J) plasma cells, displayed to show (i) proportional representation of transcript types (absolute numbers below) and (ii) the top-50 protein-coding genes ranked by corr. score, with differential expression scores (corr. with corresponding cell type *Ref.T*. panel minus max corr. with any other *Ref.T*. panel) and mean TPM expression. TEC, to be experimentally confirmed. See also Table S2, tab 1, and Figures S4 and S5.

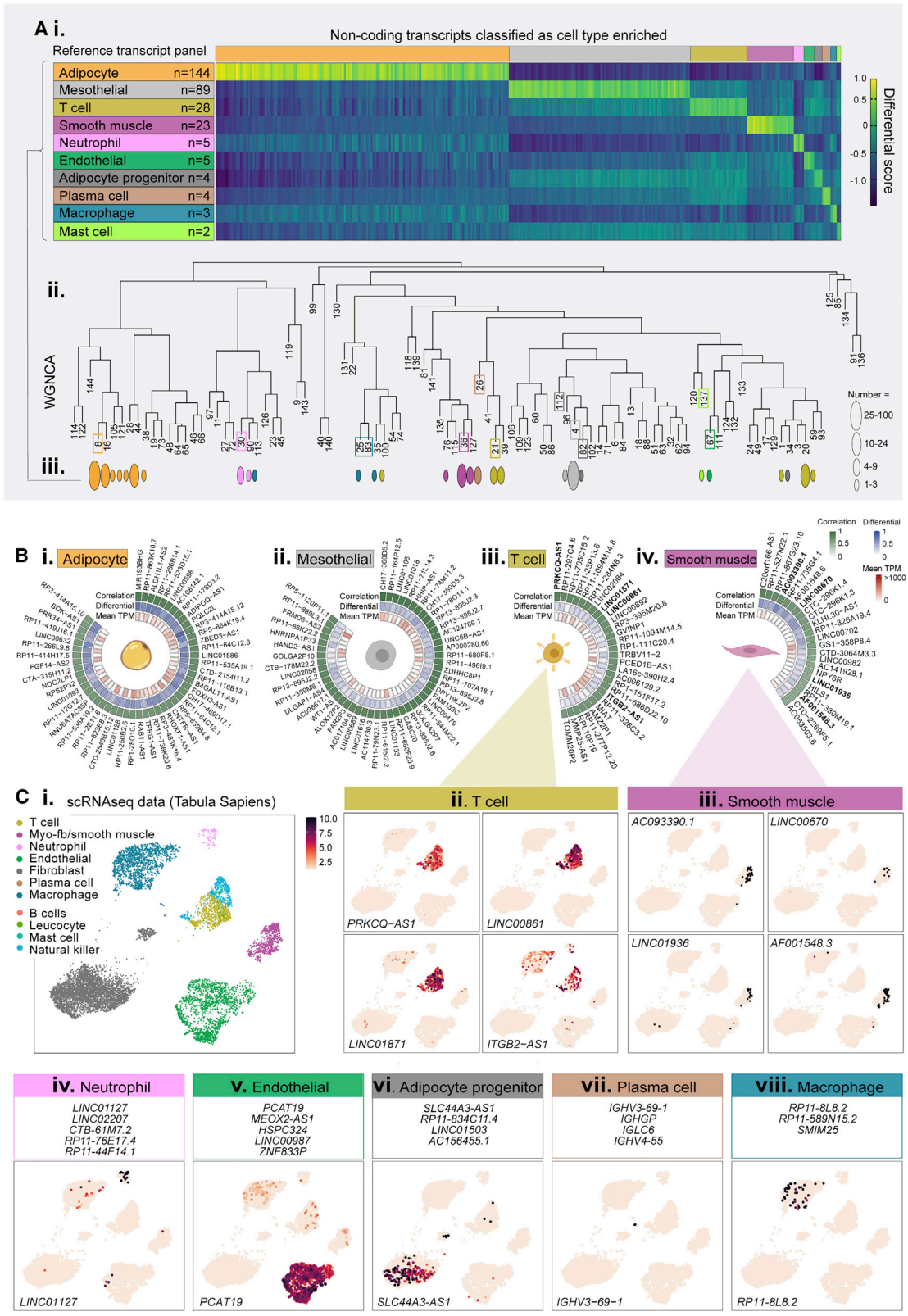

(legend on next page)

v.8 (www.gtexportal.org; Consortium, 2015). Adipocyte, adipocyte progenitor, endothelial, smooth muscle, macrophage, mast cell, T cell and plasma cell *Ref.T*.s had high intra-panel corr. (all >0.72; $p < 9.0 \times 10^{-98}$) with low inter-panel corr. (Table S1, tab 3). However, the *Ref.T*.s selected for the mesothelial cell and neutrophil panel in VAT did not correlate well with each other in SAT (mesothelial *Ref.T*. panel [mean corr. ± SD]: SAT 0.15 ± 0.04 versus VAT 0.92 ± 0.02; neutrophil *Ref.T*. panel: SAT 0.62 ± 0.08 versus VAT 0.81 ± 0.04). Expression of these genes was also much lower in SAT than VAT (mesothelial: *UPK3B* [SAT versus VAT TPM] 1.4 versus 125.8, *MSLN* 0.3 versus 144.8, *KRT19* 14.1 versus 153.4; neutrophil: *CSF3R* 0.81 versus 37.8, *FCGR3B* 2.1 versus 8.8, *CXCR2* 0.9 versus 4.6), indicating a low number, or absence, of these cell types in SAT, consistent with reports that mesothelial cells are absent (Esteve et al., 2019) and neutrophils preferentially infiltrate VAT rather than SAT (Elgazar-Carmon et al., 2008). Thus, these cell types were excluded from subsequent profiling of SAT. As for VAT, SAT cell-type-enriched transcripts were well separated by designated *Ref.T*. panels (Figure S3B) and clustered into related groups in WGCNA (Figure S3C), and terms identified by GO and reactome analysis were consistent with cell identity (Table S2, tabs 2–11, tables Bi and Bii).

Adipose tissue scRNA-seq is consistent with Ref.T. analysis

We performed a comparison between our results and scRNA-seq or small nuclear RNA-seq (snRNA-seq) data of human SAT or murine adipose tissue generated by Sun et al. (2020) (snRNA-seq), Hildreth et al. (2021), Tabula Sapiens et al. (2022), and Tabula Muris et al. (2018) (all scRNA-seq) (Table S1, tab 5). None of these studies contained all cell types we profiled; adipocytes were only in the snRNA-seq study from Sun et al. (2020) and plasma cells only in the Tabula Sapiens et al. (2022) dataset. For some cell types, e.g., progenitors, classification and/or terminology varied between studies, as is typical (Wang et al., 2021), and so comparisons were made between closely related cell types with common marker genes, e.g., "adipocyte progenitor," "pre-adipocytes," "fibroblasts," or "mesenchymal stem cells" (Table S1, tab 5 [row 2 states cell-type annotation]). For cell types represented in all, or most, of the independent studies, a high proportion of our predicted cell-type-enriched genes were elevated in the corresponding cell type in at least one (average Log2 fold change >1.0, >0.5, or >0.2 versus all other cell types [$p < 0.01$]): adipocyte progenitor (81%), endothelial cell (98%), smooth muscle cell (69%), macrophage (87%), neutrophil (96%), T cell (83%), and plasma cell (81%) enriched (Table S1, tab 5; Figures S4A and S4B). For adipocyte-enriched genes, independent validation was lowest of all cell types at 30%, which could be due to the limited coverage given by comparison with only a single study (Sun et al., 2020) or differences between the sensitivity of snRNA-seq versus bulk RNA-seq (Pimpalwar et al., 2020). Gene ontology and reactome analysis of the predicted adipocyte-enriched genes that were *not* consistent with data from Sun et al. (2020), revealed significant enrichment of terms associated with adipocyte function, e.g., "small molecule metabolic process" (adjusted FDR 8.7×10^{-29}) and "metabolism" (adjusted FDR 4.3×10^{-29}). To compare cell profiles across all datasets, we calculated the significance of overlap using a hypergeometric test (Figure S5). Genes predicted as cell-type enriched in our study were over-represented in the enriched genes in the corresponding cell types in the scRNA-seq and snRNA-seq studies (defined as those $\geq$0.5 Log2 fold change in expression versus all other cell types in the same study [$p < 0.01$]) (Figure S5), and this overlap was comparable to, or more significant than, that between the scRNA-seq and snRNA-seq studies themselves.

Ref.T. analysis can predict source of adipose-tissue-enriched genes

RNA-seq data from unfractionated human or murine tissues can be used to identify genes with enriched expression in adipose tissue versus other tissues. Adipocytes make up the majority of adipose tissue, with the most specialized function. We extracted lists of the top 200 human-adipose-tissue-enriched genes from HPA (Uhlen et al., 2015) and GTEx (Consortium, 2015), collated in the Harminozome database (Rouillard et al., 2016; Figure S4C.i). Of those genes classified as adipose tissue enriched in both datasets (n = 86), our analysis classified 66 (76.7%) as adipocyte enriched and one (1.2%) as endothelial enriched (*ARHGEF15*) (Figure S4C.ii). Thus, our analysis indicates that the majority of adipose-tissue-enriched genes are selectively expressed in adipocytes.

Sex- and depot-specific differences in adipose-cell-type transcriptome profiles

There are sex- and depot-specific differences in accumulation, distribution, endocrine, and metabolic function of adipose tissue (Blaak, 2001; Chait and den Hartigh, 2020; Lumish et al.,

Figure 4. Integrative co-expression analysis of unfractionated RNA-seq reveals enriched non-coding transcriptomes of human VAT cell types

(A) (i) Heatmap of all non-coding transcripts classified as cell type enriched (indicated by horizontal colored bars), showing differential score between mean corr. with the corresponding *Ref.T*. panel versus highest mean corr. coefficient among the other *Ref.T*. panels. (ii) Human VAT RNA-seq data (n = 527) for all sequenced transcripts were subject to WGCNA. Colored squares indicate *Ref.T*. location on resultant dendrogram (colors correspond to cell types as annotated in A.i). (iii) Colored ovals indicate distribution of non-coding transcripts classified as cell type enriched across dendrogram groups.

(B) Cell-type-enriched non-coding transcripts in (i) adipocytes, (ii) mesothelial cells, (iii) T cells, and (iv) smooth muscle cells displayed to show up to the top 50 ranked by corr. score, with differential expression scores (corr. with corresponding cell type *Ref.T*. panel minus max corr. with any other *Ref.T*. panel) and mean TPM expression.

(C) scRNA-seq data from analysis of cell types from human subcutaneous adipose tissue were sourced from Tabula Sapiens (Tabula Sapiens et al., 2022) and used to generate uniform manifold approximation and projection (UMAP) plots showing (i) scRNA-seq cell-type annotations and the expression of examples of non-coding genes we predicted as being (ii) T cell, (iii) smooth muscle cell, (iv) neutrophil, (v) endothelial, (vi) adipocyte progenitor, (vii) plasma cell, or (viii) macrophage enriched.

See also Table S2, tab 1.

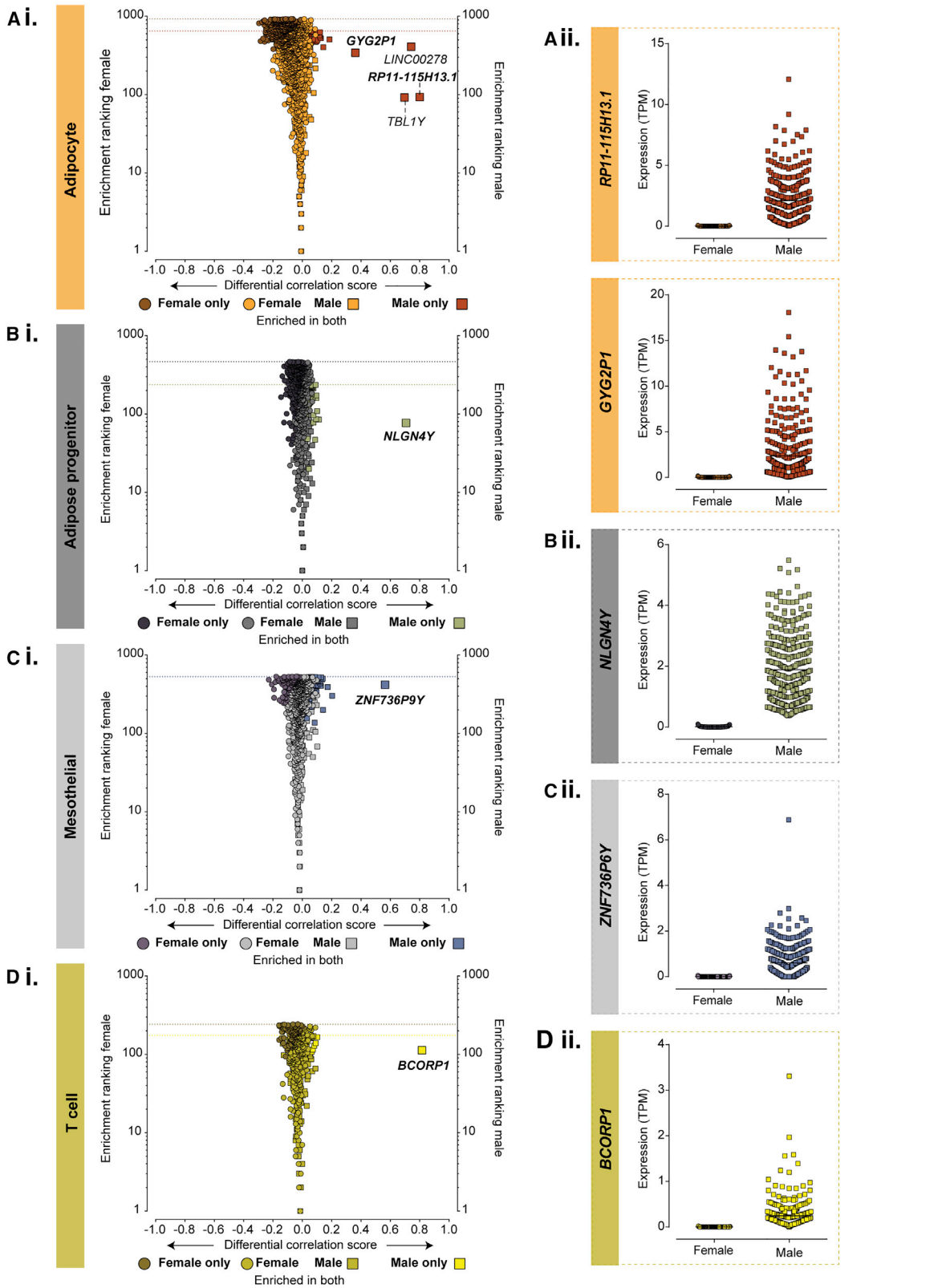

(legend on next page)

2020; Valencak et al., 2017), but to our knowledge, there are no studies describing sex- and depot-specific differences in adipose-cell-type-specific transcriptome profiles. Therefore, we profiled SAT-cell-type-enriched transcriptomes and performed a comparative sex subset analysis in VAT and SAT, and we did a comparison between cell types found in both depots.

Prediction of sex-specific differences in adipose-cell-type-enriched transcripts

We performed a subset analysis of the VAT RNA-seq dataset (female n = 165; male n = 362) to identify sex-specific, cell-type-enriched transcriptome profiles. As in the full dataset, intra-panel cell type *Ref.T*.s correlated well in female- and male-sample subsets (all >0.83; $p < 1.0 \times 10^{-33}$) (Table S3, tab 1, tables A and B). We compared transcripts classified as male or female cell type enriched (Figure 5; Table S3, tab 2). Cell profiles were largely comparable between sexes (Figures 5 and S6; transcripts enriched in *both* males and females represented by common colored circle and square symbols, respectively). Some transcripts were classified as enriched *only* in males or females (Figures 5 and S6; represented by differently colored circle and square symbols, respectively); however, most had differential corr. scores close to zero, indicating that they fell marginally below the designated threshold for classification as enriched in the other sex. A small number of markedly male-only cell-type-enriched transcripts were identified in adipocytes (Figure 5A.i; *TBL1Y*, *RP11-115H13.1*, LINC00278, and *GYG2P1*), adipocyte progenitor cells (Figure 5B.i; *NLGN4Y*), mesothelial cells (Figure 5C.i; *ZNF736P9Y*), and T cells (Figure 5D.i; *BCORP1*). In all cases, transcripts were Y linked, and mRNA expression was only detected above background levels in male VAT samples (Figures 5A.ii–5D.ii). There were no clear sex-specific differences in the other cell-enriched transcriptome profiles (Figure S6).

Comparison of predicted sex-specific VAT- and SAT-cell-type-enriched transcripts

To establish whether these sex-specific differences also existed in SAT, we performed an equivalent subset analysis of the SAT RNA-seq dataset (female n = 212; male n = 434). As in the full dataset, intra-panel cell type *Ref.T*.s correlated well in female- and male-sample subsets (all >0.71; $p < 14.0 \times 10^{-31}$) (Table S3, tab 3, tables A and B). We compared transcripts classified as male or female cell type enriched (Figures 5 and S7; Table S3, tab 4). Three out of the four transcripts we identified as adipocyte enriched in male VAT, but not female VAT, had the same profile in SAT (*TBL1Y*, *RP11-115H13.1*, and *GYG2P1*) (Figure S7A), showing consistency between adipose depot type. The single transcript we identified as adipocyte progenitor enriched in male, but not female, VAT (*NLGN4Y*) (Figure 5B.i) was not classified as such in SAT (Figure S7B). However, the corr. value between *NLGN4Y* and the adipocyte progenitor *Ref.T*. panel fell marginally below the threshold for definition as enriched in SAT, and a clear male-female differential corr. existed (SAT male corr. 0.46 versus SAT female corr. 0.10) (Table S3, tab 4). The transcript we identified as mesothelial enriched in male, but not female, VAT (*ZNF736P9Y*) (Figure 5C.i) was not expressed in SAT, consistent with the absence of mesothelial cells in this depot (Esteve et al., 2019). The male-only T cell enriched in VAT (*BCORP1*) was excluded from analysis in SAT, due to low expression in the majority of samples (>50% with TPM < 0.1). There were no clear sex-specific differences in the other SAT-cell-type-enriched transcriptome profiles (Figures S7B–S7H).

Prediction of depot-specific differences in adipose-cell-type-enriched transcripts

Previous studies have reported differential gene expression profiles between VAT and SAT depots, using bulk sequencing data (Bradford et al., 2019; Schleinitz et al., 2020), but reports on differences at the cell-type level are lacking. Here, we compared transcripts classified as cell type enriched in VAT or SAT. As we profiled two additional cell types in VAT, compared with SAT (mesothelial cells and neutrophils), prior to comparison, we excluded any SAT-cell-type-enriched transcripts that were predicted as primarily enriched in neutrophils or mesothelial cells in VAT (see Table S1, tab 6). This exclusion revealed that 79 genes were predominantly enriched in different cell types in VAT and SAT, e.g., *IL18* was classified as macrophage enriched in SAT but mesothelial-enriched in VAT (Table S1, tab 6, line 74), where its expression was higher (mean TMP ± SD; VAT 44.0 ± 41.1 versus SAT 11.8 ± 10.2). Adipocyte-enriched profiles were similar between depots, with around 500 transcripts classified as such in both VAT and SAT (Figure 6A; represented by common colored circle and square symbols, respectively) (Table S2, tab 1). *LINC01632* and *GPAT3* were classified as adipocyte enriched in VAT only (Figure 6A), and both were expressed at higher levels in VAT than SAT (Figures 6C.i and 6C.ii). Conversely, *NRCAM*, *MAGI2-AS3*, and *SEPT11* were classified as adipocyte enriched in SAT only (Figure 6A) and were all expressed at higher levels in SAT than VAT (Figures 6C.iii–6C.v). These data are consistent with these transcripts having both an adipocyte-restricted and depot-restricted profile. Glucagon-like peptide-2 receptor (*GLP2R*) was classified as adipocyte enriched in SAT only (Figure 6A), but it was expressed at higher levels in VAT (mean TMP ± STD; VAT 11.2 ± 11.28 versus SAT 1.37 ± 0.85). This gene could be strongly

Figure 5. Identification of sex-specific, cell-enriched transcripts in human VAT

VAT RNA-seq data (n = 527 individuals) were divided into female and male subgroups (female n = 165; male n = 362) before classification of cell-type-enriched transcripts. For transcripts classified as (A.i) adipocyte, (B.i) adipocyte progenitor, (C.i) mesothelial, or (D.i) T cell enriched, in either sex, the "sex differential corr. score" (difference between mean corr. with the *Ref.T*. panel in females versus males) was plotted versus "enrichment ranking" (position in each respective enriched list; highest corr. = rank 1). On each plot, transcripts enriched in *both* females and males are represented by common colored circle and square symbols, respectively, and transcripts classified as enriched *only* in females or males are represented by differently colored circle and square symbols, respectively. Expression in female and male samples for transcripts identified as male-only enriched in (A.ii) adipocytes, (B.ii) adipocyte progenitor, (C.ii) mesothelial, or (D.ii) T cells. See also Figure S6 and Table S3.

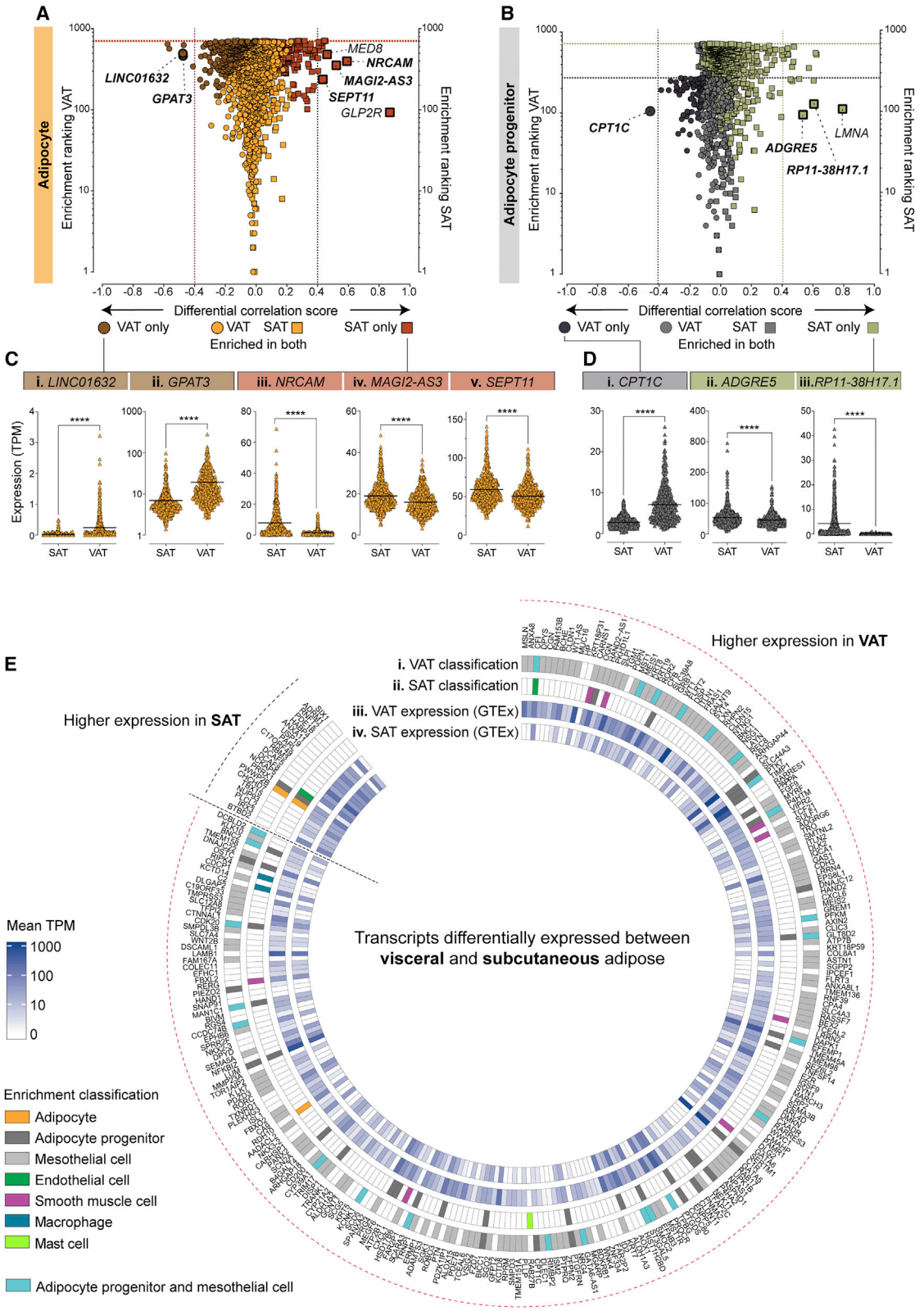

(legend on next page)

transcriptionally regulated by environmental factors, analogous to regulation of the related glucagon receptor gene in response to glucose (Svoboda et al., 1999), in VAT only and thus here does not consistently correlate with the stably expressed adipocyte *Ref. T*. Like adipocytes, adipocyte-progenitor-enriched profiles were similar between depots, with 186 transcripts classified as such in both VAT and SAT (Figure 6B; represented by common colored circle and square symbols, respectively) (Table S2, tab 1). *CPT1C* was classified as adipocyte progenitor enriched in VAT only (Figure 6B) and expressed at higher levels in VAT than SAT (Figure 6D.i). Conversely, *ADGRE5* and *RP11-38H17.1* were classified as adipocyte progenitor enriched in SAT only (Figure 6B) and were expressed at higher levels in SAT than VAT (Figures 6D.ii and 6D.iii). These data are consistent with these transcripts having both an adipocyte-progenitor-restricted and depot-restricted profile. There were no clear depot-specific differences in the other cell-type-enriched transcriptome profiles (Figures S8A–S8F).

As our analysis indicated that cell-type-enrichment profiles did not differ substantially in VAT and SAT, we investigated the cell-type-expression profile of genes identified as most differentially expressed between depots. We extracted data from a study (Schleinitz et al., 2020) where the authors analyzed samples from 15 human-fat depots and generated a list of most differentially expressed genes between SAT and VAT. Of the 298 transcripts identified by the authors, data for 272 were available in our analysis. We performed lookups in our dataset to determine whether these genes were classified cell type enriched and whether this expression profile differed between VAT and SAT (Figure 6E). For transcripts with a higher expression in VAT, compared with SAT (Schleinitz et al., 2020; Figure 6E, indicated by red dashed external line), the majority were classified as mesothelial cell enriched in VAT in our analysis (Figure 6E.i), a cell type not found in SAT (Esteve et al., 2019). A further 25 of these transcripts were found in the list of 84 we excluded from cell-type classification, due to likely co-expression in both VAT mesothelial and adipocyte progenitor cells (Figure 6E.i; Table S1, tab 4a). For those transcripts with a higher expression in SAT versus VAT (Schleinitz et al., 2020; Figure 6E, indicated by black dashed line), most were not annotated as cell type enriched, but those that were had similar expression profiles between depots. Classification as depot enriched in Schleinitz et al. (2020) was broadly consistent with corresponding TPMs in the GTEx data (Figures 6E.iii and 6E.iv). The application of our data in this way demonstrates its usefulness for extracting cell-type information from whole-tissue data, allowing further understanding of observations made in other studies, with broad applicability across datasets and analysis platforms.

DISCUSSION

Here, we present a method to resolve unfractionated tissue RNA-seq data, providing an alternative to scRNA-seq for the identification of cell-type-enriched transcripts. Our approach circumvents some challenges associated with scRNA-seq, e.g., requirement for fresh tissue, artefact-generating sample preprocessing, and limited read depth (Beliakova-Bethell et al., 2014; Rizzetto et al., 2017; Saliba et al., 2014; Ziegenhain et al., 2017). By analyzing a high number of biological replicates, this approach allows for well-powered subgroup comparisons, e.g., female versus male. Public repositories contain thousands of bulk RNA-seq datasets; our method can utilize these resources to profile cell types for which little or no information currently exists.

To our knowledge, this study provides the most comprehensive publicly accessible database of adipose-tissue-cell-type coding and non-coding gene-expression-enrichment profiles, searchable on a gene-by-gene basis. Our dataset could also be a useful tool for the optimization of deconvolution algorithms used to determine proportions of constituent cell types in adipose tissue bulk RNA-seq, e.g., CIBERSORT (Glastonbury et al., 2019; Newman et al., 2015). Such analyses typically use input expression matrices generated from transcriptome analysis of isolated cell types to identify cell-type reference genes. Various factors can reduce the accuracy of input matrices, including contaminating cell types in input datasets, technical artefacts due to cell extraction and processing, and limited input data availability for some cell types or for cells sourced from adipose tissue. Cross checking input matrices against our dataset could identify the most likely highly enriched genes *in vivo*.

Genes classified as adipocyte enriched in VAT or SAT included those with established roles in adipocyte development or function, e.g., *GPD1*, *AQP7*, *LPL* (Rotondo et al., 2017), *CIDEC* (Keller et al., 2008), *GYG2*, *TUSC5*, and *PPP1R1A* (Ambele et al., 2016), but others had no known function, e.g., *HEPACAM*, *PECR*, *C19orf12*, and AL845331.1. *HEPACAM* encodes an adhesion molecule studied mainly in brain glial cells (Barrallo-Gimeno and Estevez, 2014), but it was identified as a key driver in a regulatory gene network associated with BMI and cholesterol in VAT from patients with coronary artery disease (Franzen et al., 2016). *HEPACAM* was one of 47 genes differentially expressed in SAT

Figure 6. Identification of depot-specific, cell-enriched transcripts in human adipose tissue

Human VAT (n = 527 individuals) or SAT (n = 646 individuals) RNA-seq data were used for classification of cell-type-enriched transcripts (see results for criteria).

(A and B) For transcripts classified as (A) adipocyte or (B) adipocyte progenitor enriched, in either VAT or SAT, the "depot differential corr. score" (difference between mean corr. with the *Ref.T*. panel in VAT versus SAT) was plotted versus enrichment ranking (position in each respective enriched list; highest corr. = rank 1). On each plot, transcripts enriched in *both* VAT and SAT are represented by common colored circle and square symbols, respectively, and transcripts classified as enriched *only* in VAT or SAT are represented by differently colored circle or square symbols, respectively. Correspondingly colored threshold lines denote ranking below which transcripts were classified as VAT or SAT enriched.

(C and D) Expression levels in SAT and VAT of (C) transcripts classified as adipocyte enriched in (i and ii) VAT only or (iii–v) SAT only; (D) adipocyte progenitor-enriched classified transcripts in (i) VAT only or (ii and iii) SAT only.

(E) Transcripts identified as differentially expressed between VAT and SAT depots by Schleinitz et al. (2020) are displayed with cell-type-enrichment classification in our analysis of (i) VAT and (ii) SAT. Corresponding expression levels in the GTEx datasets are displayed for (iii) VAT and (iv) SAT.

See also Figure S8 and Tables S1, tab 6, and S2.

from twin pairs with high and low BMI and was associated with adipocyte diameter (Kaartinen et al., 2020). *PECR* is involved in chain elongation of fatty acids (Gloerich et al., 2006) and is a candidate gene influencing fat mass in mice (Karst et al., 2011), intramuscular fat deposition in cows (Sadkowski et al., 2014), and pig weight (Stuczynska et al., 2018). Mutations in *C19orf12* cause neurodegeneration with brain iron accumulation (Gagliardi et al., 2015), and *C19orf12* could have a role in lipid homeostasis (Hartig et al., 2011), due to high expression in adipose tissue and co-regulation with genes involved in fatty-acid metabolism. *AL845331.1* has been re-classified from non-coding to novel protein coding, on the basis of its similarity to *AQP7*, a gene we also classified as adipocyte enriched, as have others (Rotondo et al., 2017).

Non-coding RNAs are increasingly recognized as important in adipose biology (Squillaro et al., 2020; Statello et al., 2021; Xu and Sun, 2020), but descriptions of adipose-cell-type expression profiles are lacking. In our analysis, adipocytes had the most enriched non-coding genes, including antisense transcripts to adipocyte-enriched protein-coding genes, e.g., *ALDH1L1-AS2*, *ADIPOQ-AS1*, *LIPE-AS1*, and *CNTFR-AS1*. Other adipocyte-enriched non-coding genes included *RP11-863K10.7*, an antisense transcript to *ERLIN2*, a gene with a role in the accumulation of cytosolic lipid droplets (Wang et al., 2012); *MIRLET7BHG*, which is important for adipocyte differentiation in mice (McGregor and Choi, 2011; Sun et al., 2009); and *MIR193BHG*, which was characterized as a cellular steroid biosynthesis pathway modulator in MCF7 cells (Wu et al., 2020). Mesothelial-cell-enriched non-coding genes included antisense transcripts to mesothelial-enriched protein-coding genes, e.g., *SEMA3B-AS*, *DPP10-AS1*, *FAM83H-AS1*, and *WT1-AS1*. Other mesothelial-enriched non-coding genes included *LINC01133*, reported as having a role in the Wnt signaling pathway (Yang et al., 2021), which is associated with metabolic disease development, with adipose depot-specific roles (Chen and Wang, 2018). Most non-coding transcripts classified as T cell or plasma cell enriched in our analysis were TR genes or IG genes, respectively. Other non-coding transcripts classified as T cell enriched included *PRKCQ-AS1*, which was postulated to have a role in T cell function in a study of lncRNAs in vaccine response (de Lima et al., 2019) and targets the protein-coding gene *PRKCQ*, which was also classified as T cell enriched in our analysis. However, the majority of non-coding transcripts we identified as cell type enriched are uncharacterized.

Sex differences in the accumulation, distribution, and endocrine and metabolic function of adipose tissue is well acknowledged (Blaak, 2001; Lumish et al., 2020; Valencak et al., 2017), although studies on underlying cell-type gene-expression differences are limited. Cell-type profiles were similar between sexes, but we did identify a small panel of transcripts with sex-dependent enrichment profiles, including *TBL1Y*, *GYG2P1*, and *RP11-115H13.1*, which were adipocyte enriched only in male VAT and SAT. *TBL1Y*, a Y-linked gene similar to its gonosomal homologue *TBL1X*, is one of 27 genes that encode distinct male-specific Y proteins (Jeffery et al., 2013). *TBL1Y* has a role in hereditary hearing loss (Di Stazio et al., 2019) and cardiac developmental regulation (Meyfour et al., 2017), the latter of which has been suggested to contribute to the sexual dimorphism of cardiac diseases. Although previously reported as expressed in adipose tissue (Jeffery et al., 2013), there are no reports of *TBL1Y* being adipocyte specific or its function there. *GYG2P1* is a Y-linked pseudogene of *GYG2* (Meyfour et al., 2017). *GYG2* was classified as adipocyte enriched in both males and females in our analysis; although its function in adipocytes has not been studied, its expression coincides with adipocyte maturation of adipose-derived stromal cells (Ambele et al., 2016). Although pseudogenes are often assumed to lack function, they are increasingly found to have key roles (Cheetham et al., 2020) functioning as antisense, endogenous small-interference or competing endogenous transcripts (Singh et al., 2020). There are no reports of *GYG2P1* function, but it was downregulated in SAT from children with obesity versus those without (Liu et al., 2018). A recent study used bulk RNA-seq to analyze SAT from females and males to identify genes with differential expression (Anderson et al., 2020). According to our data, the identified genes had similar cell-type enrichment profiles between sexes (majority adipocyte enriched). Thus, sex differences in SAT are likely driven by variable gene expression in a common cell type or differences in the proportion of this cell type.

Previous studies have identified differences in cellular composition, adipocyte size, activity, and capacity for fat uptake between VAT and SAT (Ibrahim, 2010). Although RNA-seq has been used to determine differences in gene expression between VAT and SAT (Bradford et al., 2019; Schleinitz et al., 2020), to our knowledge, there have been no studies comparing cell-type-enriched transcriptome profiles. We found that *NRCAM*, a neuronal cell adhesion molecule of the immunoglobulin superfamily, mainly studied in a neuronal development (Sakurai, 2012), was adipocyte enriched in SAT, but not VAT. *NRCAM* was one of 32 genes upregulated throughout the differentiation of human-adipose-derived stromal cells isolated from SAT (Ambele et al., 2016), and in a study of SAT from siblings with high and low BMI, *NRCAM* was identified as part of an obesity-related transcript network (Walley et al., 2012). *NRCAM* was expressed in SAT, but not VAT, from individuals with extreme obesity (Gerhard et al., 2014). However, *NRCAM* function is unknown. In SAT, but not VAT, *CALB2* and *PKP2* were adipocyte enriched and *IL18* was macrophage enriched. In all three cases, overall expression was higher in VAT than SAT, and these genes were predominantly expressed in mesothelial cells in VAT, consistent with previous reports for *IL18* (Darimont et al., 2008) and *CALB2* (Barberis et al., 1997). Indeed, our data show that mesothelial cells in VAT drive differences in global gene expression between depots (Bradford et al., 2019; Schleinitz et al., 2020).

In summary, our method circumvents some challenges associated with the analysis of adipose tissue to provide an atlas of constituent cell type defining transcriptional profiles. The data can be used to further interpretate existing observations and to identify candidates for functional studies to expand our knowledge of adipose tissue in health and disease.

Limitations of the study

There are limitations to our study. We do not profile specific cell subtypes; while it may be possible to resolve the data further in this way, there is a lack of consensus regarding cell-subtype

identity, e.g., multiple adipocyte progenitor cells subtypes have been reported (Raajendiran et al., 2019), but others claim this population is homogeneous (Acosta et al., 2017). Thus, selection of subtype *Ref.T*.s required for input into our analysis model, or interpretation of WGNCA, is challenging. Thus, our classification informs about cell-type restricted expression but does not discriminate between transcripts expressed uniformly across all cells of a given type and those expressed in a sub-population. Some cell types are not profiled in our analysis, due to difficulties in the identification of cell-type-specific markers as suitable *Ref.T*.s. Thus, some genes classified as cell type enriched in our analysis may also be expressed in other (non-profiled) cell types, a limitation that applies to existing scRNA-seq and snRNA-seq adipose tissue datasets, which all lack data for some constituent cell types (e.g., Hildreth et al., 2021; Tabula Muris et al., 2018; Tabula Sapiens et al., 2022; Vijay et al., 2020). Expression of some genes in adipose tissue can be modified by genetic, epigenetic, or environmental factors (Sun et al., 2019). Such genes may not correlate with the *Ref.T*.s, due to a variation in expression that is independent of cell-type proportions. Thus, such genes could be false negatives in our analysis. We have used high thresholds for classification of genes as cell type enriched, likely leading to the incorrect exclusion of some. For example, *EPAS1*, *SHROOM4*, and *GPR4* are endothelial-enriched transcripts across tissue beds (Butler et al., 2016), but they fall just below the threshold for classification as endothelial enriched here. However, in these cases, the enrichment score clearly indicates a cell-type-restricted expression; thus, our classifications are intended only as a guide, and the reader should consider the data on a transcript-by-transcript basis.

STAR★METHODS

Detailed methods are provided in the online version of this paper and include the following:

- KEY RESOURCES TABLE
- RESOURCE AVAILABILITY
  - Lead contact
  - Materials availability
  - Data and code availability
- EXPERIMENTAL MODEL AND SUBJECT DETAILS
- METHOD DETAILS
  - Tissue profiling: human tissue sections
- QUANTIFICATION AND STATISTICAL ANALYSIS
  - Reference transcript-based correlation analysis
  - Weighted correlation network (WGCNA) analysis
  - Gene ontology and reactome analysis
  - Processing of data from adipose tissue scRNA-seq and snRNA-seq datasets
  - Visualization
- ADDITIONAL RESOURCES

SUPPLEMENTAL INFORMATION

Supplemental information can be found online at https://doi.org/10.1016/j.celrep.2022.111046.

ACKNOWLEDGMENTS

Funding was granted to L.M.B. from Hjärt Lungfonden (20170759, 20170537, and 20200544) and Swedish Research Council (2019–01493) and to J.O. from Stockholm County Council (SLL 2017–0842). The Human Protein Atlas is funded by The Knut and Alice Wallenberg Foundation. We used data from Genotype-Tissue Expression (GTEx) Project (gtexportal.org) (Consortium, 2015), supported by the Office of the Director of the National Institutes of Health and by NCI, NHGRI, NHLBI, NIDA, NIMH, and NINDS.

AUTHOR CONTRIBUTIONS

Conceptualization, L.M.B.; methodology, M.N.-T., E.C.S., S.Ö., and P.J.D.; formal analysis, M.N.-T.; investigation, M.N.-T., P.J.D., L.M.B., and C.L.; resources, M.U., F.P., J.O., L.M.B., and C.L.; writing – original draft, M.N.-T. and L.M.B.; writing – review & editing, all; visualization, M.N.-T., L.M.B., P.J.D., M.Z., and K.V.F.; supervision, L.M.B. and P.J.D.; funding acquisition, L.M.B. and J.O.

DECLARATION OF INTERESTS

The authors declare no competing interests.

Received: August 30, 2021
Revised: April 29, 2022
Accepted: June 13, 2022
Published: July 12, 2022

REFERENCES

Acosta, J.R., Joost, S., Karlsson, K., Ehrlund, A., Li, X., Aouadi, M., Kasper, M., Arner, P., Rydén, M., and Laurencikiene, J. (2017). Single cell transcriptomics suggest that human adipocyte progenitor cells constitute a homogeneous cell population. Stem Cell Res. Ther. *8*, 250. https://doi.org/10.1186/s13287-017-0701-4.

Ambele, M.A., Dessels, C., Durandt, C., and Pepper, M.S. (2016). Genome-wide analysis of gene expression during adipogenesis in human adipose-derived stromal cells reveals novel patterns of gene expression during adipocyte differentiation. Stem Cell Res. *16*, 725–734. https://doi.org/10.1016/j.scr.2016.04.011.

Anderson, W.D., Soh, J.Y., Innis, S.E., Dimanche, A., Ma, L., Langefeld, C.D., Comeau, M.E., Das, S.K., Schadt, E.E., Björkegren, J.L., and Civelek, M. (2020). Sex differences in human adipose tissue gene expression and genetic regulation involve adipogenesis. Genome Res. *30*, 1379–1392. https://doi.org/10.1101/gr.264614.120.

Armulik, A., Genové, G., and Betsholtz, C. (2011). Pericytes: developmental, physiological, and pathological perspectives, problems, and promises. Dev. Cell *21*, 193–215. https://doi.org/10.1016/j.devcel.2011.07.001.

Ashburner, M., Ball, C.A., Blake, J.A., Botstein, D., Butler, H., Cherry, J.M., Davis, A.P., Dolinski, K., Dwight, S.S., Eppig, J.T., et al. (2000). Gene Ontology: tool for the unification of biology. Nat. Genet. *25*, 25–29. https://doi.org/10.1038/75556.

Barberis, M.C., Faleri, M., Veronese, S., Casadio, C., and Viale, G. (1997). Calretinin. Acta Cytol. *41*, 1757–1761. https://doi.org/10.1159/000333181.

Barrallo-Gimeno, A., and Estevez, R. (2014). GlialCAM, a glial cell adhesion molecule implicated in neurological disease. Adv. Neurobiol. *8*, 47–59. https://doi.org/10.1007/978-1-4614-8090-7_3.

Beliakova-Bethell, N., Massanella, M., White, C., Lada, S.M., Du, P., Vaida, F., Blanco, J., Spina, C.A., and Woelk, C.H. (2014). The effect of cell subset isolation method on gene expression in leukocytes. Cytometry *85*, 94–104. https://doi.org/10.1002/cyto.a.22352.

Blaak, E. (2001). Gender differences in fat metabolism. Curr. Opin. Clin. Nutr. Metab. Care *4*, 499–502. https://doi.org/10.1097/00075197-200111000-00006.

Bradford, S.T., Nair, S.S., Statham, A.L., van Dijk, S.J., Peters, T.J., Anwar, F., French, H.J., von Martels, J.Z.H., Sutcliffe, B., Maddugoda, M.P., et al. (2019). Methylome and transcriptome maps of human visceral and subcutaneous adipocytes reveal key epigenetic differences at developmental genes. Sci. Rep. *9*, 9511. https://doi.org/10.1038/s41598-019-45777-w.

Britton, K.A., Massaro, J.M., Murabito, J.M., Kreger, B.E., Hoffmann, U., and Fox, C.S. (2013). Body fat distribution, incident cardiovascular disease, cancer, and all-cause mortality. J. Am. Coll. Cardiol. *62*, 921–925. https://doi.org/10.1016/j.jacc.2013.06.027.

Butler, L.M., Hallström, B., Fagerberg, L., Pontén, F., Ponten, F., Uhlén, M., Uhlen, M., Renné, T., and Odeberg, J. (2016). Analysis of body-wide unfractionated tissue data to identify a core human endothelial transcriptome. Cell Syst. *3*, 287–301.e3. https://doi.org/10.1016/j.cels.2016.08.001.

Chait, A., and den Hartigh, L.J. (2020). Adipose tissue distribution, inflammation and its metabolic consequences, including diabetes and cardiovascular disease. Front. Cardiovasc. Med *7*, 22. https://doi.org/10.3389/fcvm.2020.00022.

Cheetham, S.W., Faulkner, G.J., and Dinger, M.E. (2020). Overcoming challenges and dogmas to understand the functions of pseudogenes. Nat. Rev. Genet. *21*, 191–201. https://doi.org/10.1038/s41576-019-0196-1.

Chen, N., and Wang, J. (2018). Wnt/β-Catenin signaling and obesity. Front. Physiol. *9*, 792. https://doi.org/10.3389/fphys.2018.00792.

Consortium, G.T. (2015). Human genomics. The Genotype-Tissue Expression (GTEx) pilot analysis: multitissue gene regulation in humans. Science *348*, 648–660. https://doi.org/10.1126/science.1262110.

Darimont, C., Avanti, O., Blancher, F., Wagniere, S., Mansourian, R., Zbinden, I., Leone-Vautravers, P., Fuerholz, A., Giusti, V., Giusti, V., et al. (2008). Contribution of mesothelial cells in the expression of inflammatory-related factors in omental adipose tissue of obese subjects. Int. J. Obes. *32*, 112–120. https://doi.org/10.1038/sj.ijo.0803688.

de Lima, D.S., Cardozo, L.E., Maracaja-Coutinho, V., Suhrbier, A., Mane, K., Jeffries, D., Silveira, E.L.V., Amaral, P.P., Rappuoli, R., de Silva, T.I., and Nakaya, H.I. (2019). Long noncoding RNAs are involved in multiple immunological pathways in response to vaccination. Proc. Natl. Acad. Sci. USA *116*, 17121–17126. https://doi.org/10.1073/pnas.1822046116.

Di Stazio, M., Collesi, C., Vozzi, D., Liu, W., Myers, M., Morgan, A., D'Adamo, P.A., Girotto, G., Rubinato, E., Giacca, M., and Gasparini, P. (2019). TBL1Y: a new gene involved in syndromic hearing loss. Eur. J. Hum. Genet. *27*, 466–474. https://doi.org/10.1038/s41431-018-0282-4.

Dusart, P., Hallström, B.M., Renné, T., Odeberg, J., Uhlén, M., and Butler, L.M. (2019). A systems-based map of human brain cell-type enriched genes and malignancy-associated endothelial changes. Cell Rep. *29*, 1690–1706.e4. https://doi.org/10.1016/j.celrep.2019.09.088.

Elgazar-Carmon, V., Rudich, A., Hadad, N., and Levy, R. (2008). Neutrophils transiently infiltrate intra-abdominal fat early in the course of high-fat feeding. J. Lipid Res. *49*, 1894–1903. https://doi.org/10.1194/jlr.m800132-jlr200.

Estève, D., Boulet, N., Belles, C., Zakaroff-Girard, A., Decaunes, P., Briot, A., Veeranagouda, Y., Didier, M., Remaury, A., Guillemot, J.C., et al. (2019). Lobular architecture of human adipose tissue defines the niche and fate of progenitor cells. Nat. Commun. *10*, 2549. https://doi.org/10.1038/s41467-019-09992-3.

Franzén, O., Ermel, R., Cohain, A., Akers, N.K., Di Narzo, A., Talukdar, H.A., Foroughi-Asl, H., Giambartolomei, C., Fullard, J.F., Sukhavasi, K., et al. (2016). Cardiometabolic risk loci share downstream cis- and trans-gene regulation across tissues and diseases. Science *353*, 827–830. https://doi.org/10.1126/science.aad6970.

Franzen, O., Gan, L.M., and Bjorkegren, J.L.M. (2019). PanglaoDB: A Web Server for Exploration of Mouse and Human Single-Cell RNA Sequencing Data (Database).

Gagliardi, M., Annesi, G., Lesca, G., Broussolle, E., Iannello, G., Vaiti, V., Gambardella, A., and Quattrone, A. (2015). C19orf12 gene mutations in patients with neurodegeneration with brain iron accumulation. Park. Relat. Disord. *21*, 813–816. https://doi.org/10.1016/j.parkreldis.2015.04.009.

Gene Ontology Consortium (2021). The Gene Ontology resource: enriching a GOld mine. Nucleic Acids Res. *49*, D325–D334. https://doi.org/10.1093/nar/gkaa1113.

Gerhard, G.S., Styer, A.M., Strodel, W.E., Roesch, S.L., Yavorek, A., Carey, D.J., Wood, G.C., Petrick, A.T., Gabrielsen, J., Gabrielsen, J., et al. (2014). Gene expression profiling in subcutaneous, visceral and epigastric adipose tissues of patients with extreme obesity. Int. J. Obes. *38*, 371–378. https://doi.org/10.1038/ijo.2013.152.

Glastonbury, C.A., Couto Alves, A., El-Sayed Moustafa, J.S., and Small, K.S. (2019). Cell-type heterogeneity in adipose tissue is associated with complex traits and reveals disease-relevant cell-specific eQTLs. Am. J. Hum. Genet. *104*, 1013–1024. https://doi.org/10.1016/j.ajhg.2019.03.025.

Gloerich, J., Ruiter, J.P., van den Brink, D.M., Ofman, R., Ferdinandusse, S., and Wanders, R.J. (2006). Peroxisomal trans-2-enoyl-CoA reductase is involved in phytol degradation. FEBS Lett. *580*, 2092–2096. https://doi.org/10.1016/j.febslet.2006.03.011.

Gu, Z., Gu, L., Eils, R., Schlesner, M., and Brors, B. (2014). Circlize Implements and enhances circular visualization in R. Bioinformatics *30*, 2811–2812. https://doi.org/10.1093/bioinformatics/btu393.

Han, X., Zhou, Z., Fei, L., Sun, H., Wang, R., Chen, Y., Chen, H., Wang, J., Tang, H., Ge, W., et al. (2020). Construction of a human cell landscape at single-cell level. Nature *581*, 303–309. https://doi.org/10.1038/s41586-020-2157-4.

Hao, Y., Hao, S., Andersen-Nissen, E., Mauck, W.M., 3rd, Zheng, S., Butler, A., Lee, M.J., Wilk, A.J., Darby, C., Zager, M., et al. (2021). Integrated analysis of multimodal single-cell data. Cell *184*, 3573–3587.e29. https://doi.org/10.1016/j.cell.2021.04.048.

Harrow, J.L., Steward, C.A., Frankish, A., Gilbert, J.G., Gonzalez, J.M., Loveland, J.E., Mudge, J., Sheppard, D., Thomas, M., Trevanion, S., and Wilming, L.G. (2014). The vertebrate genome annotation browser 10 years on. Nucleic Acids Res. *42*, D771–D779. https://doi.org/10.1093/nar/gkt1241.

Hartig, M.B., Iuso, A., Haack, T., Kmiec, T., Jurkiewicz, E., Heim, K., Roeber, S., Tarabin, V., Dusi, S., Krajewska-Walasek, M., et al. (2011). Absence of an orphan mitochondrial protein, c19orf12, causes a distinct clinical subtype of neurodegeneration with brain iron accumulation. Am. J. Hum. Genet. *89*, 543–550. https://doi.org/10.1016/j.ajhg.2011.09.007.

Hildreth, A.D., Ma, F., Wong, Y.Y., Sun, R., Pellegrini, M., and O'Sullivan, T.E. (2021). Single-cell sequencing of human white adipose tissue identifies new cell states in health and obesity. Nat. Immunol. *22*, 639–653. https://doi.org/10.1038/s41590-021-00922-4.

Hilgendorf, K.I. (2021). Primary cilia are critical regulators of white adipose tissue expansion. Front. Physiol. *12*, 769367. https://doi.org/10.3389/fphys.2021.769367.

Hu, E., Liang, P., and Spiegelman, B.M. (1996). AdipoQ is a novel adipose-specific gene dysregulated in obesity. J. Biol. Chem. *271*, 10697–10703. https://doi.org/10.1074/jbc.271.18.10697.

Ibrahim, M.M. (2010). Subcutaneous and visceral adipose tissue: structural and functional differences. Obes. Rev. *11*, 11–18. https://doi.org/10.1111/j.1467-789x.2009.00623.x.

Jeffery, H.C., Söderberg-Naucler, C., and Butler, L.M. (2013). Human cytomegalovirus induces a biphasic inflammatory response in primary endothelial cells. J. Virol. *87*, 6530–6535. https://doi.org/10.1128/jvi.00265-13.

Kaartinen, M.T., Arora, M., Heinonen, S., Rissanen, A., Kaprio, J., and Pietiläinen, K.H. (2020). Transglutaminases and obesity in humans: association of F13A1 to adipocyte hypertrophy and adipose tissue immune response. Int. J. Mol. Sci. *21*, 8289. https://doi.org/10.3390/ijms21218289.

Kahn, C.R., Wang, G., and Lee, K.Y. (2019). Altered adipose tissue and adipocyte function in the pathogenesis of metabolic syndrome. J. Clin. Invest. *129*, 3990–4000. https://doi.org/10.1172/jci129187.

Karlsson, M., Zhang, C., Méar, L., Zhong, W., Digre, A., Katona, B., Sjöstedt, E., Butler, L., Odeberg, J., Dusart, P., et al. (2021). A single–cell type transcriptomics map of human tissues. Sci. Adv. *7*, eabh2169. https://doi.org/10.1126/sciadv.abh2169.

Kärst, S., Cheng, R., Schmitt, A.O., Yang, H., de Villena, F.P.M., Palmer, A.A., and Brockmann, G.A. (2011). Genetic determinants for intramuscular fat content and water-holding capacity in mice selected for high muscle mass. Mamm. Genome *22*, 530–543. https://doi.org/10.1007/s00335-011-9342-6.

Keller, P., Petrie, J.T., De Rose, P., Gerin, I., Wright, W.S., Chiang, S.H., Nielsen, A.R., Fischer, C.P., Pedersen, B.K., and MacDougald, O.A. (2008). Fat-specific protein 27 regulates storage of triacylglycerol. J. Biol. Chem. *283*, 14355–14365. https://doi.org/10.1074/jbc.m708323200.

Langfelder, P., and Horvath, S. (2008). WGCNA: an R package for weighted correlation network analysis. BMC Bioinf. *9*, 559. https://doi.org/10.1186/1471-2105-9-559.

Liu, Y., Ji, Y., Li, M., Wang, M., Yi, X., Yin, C., Wang, S., Zhang, M., Zhao, Z., and Xiao, Y. (2018). Integrated analysis of long noncoding RNA and mRNA expression profile in children with obesity by microarray analysis. Sci. Rep. *8*, 8750. https://doi.org/10.1038/s41598-018-27113-w.

Lu, J., Zhao, J., Meng, H., and Zhang, X. (2019). Adipose tissue-resident immune cells in obesity and type 2 diabetes. Front. Immunol. *10*, 1173. https://doi.org/10.3389/fimmu.2019.01173.

Lumish, H.S., O'Reilly, M., and Reilly, M.P. (2020). Sex differences in genomic drivers of adipose distribution and related cardiometabolic disorders: opportunities for precision medicine. Arterioscler. Thromb. Vasc. Biol. *40*, 45–60. https://doi.org/10.1161/atvbaha.119.313154.

Martinez, F.O., Gordon, S., Locati, M., and Mantovani, A. (2006). Transcriptional profiling of the human monocyte-to-macrophage differentiation and polarization: new molecules and patterns of gene expression. J. Immunol. *177*, 7303–7311. https://doi.org/10.4049/jimmunol.177.10.7303.

A McGregor, R., and S Choi, M. (2011). microRNAs in the regulation of adipogenesis and obesity. Curr. Mol. Med. *11*, 304–316. https://doi.org/10.2174/156652411795677990.

Meyfour, A., Ansari, H., Pahlavan, S., Mirshahvaladi, S., Rezaei-Tavirani, M., Gourabi, H., Baharvand, H., and Salekdeh, G.H. (2017). Y chromosome missing protein, TBL1Y, may play an important role in cardiac differentiation. J. Proteome Res. *16*, 4391–4402. https://doi.org/10.1021/acs.jproteome.7b00391.

Mi, H., Muruganujan, A., Casagrande, J.T., and Thomas, P.D. (2013). Large-scale gene function analysis with the PANTHER classification system. Nat. Protoc. *8*, 1551–1566. https://doi.org/10.1038/nprot.2013.092.

Mi, H., Poudel, S., Muruganujan, A., Casagrande, J.T., and Thomas, P.D. (2016). PANTHER version 10: expanded protein families and functions, and analysis tools. Nucleic Acids Res. *44*, D336–D342. https://doi.org/10.1093/nar/gkv1194.

Min, S.Y., Desai, A., Yang, Z., Sharma, A., DeSouza, T., Genga, R.M.J., Kucukural, A., Lifshitz, L.M., Nielsen, S., Scheele, C., et al. (2019). Diverse repertoire of human adipocyte subtypes develops from transcriptionally distinct mesenchymal progenitor cells. Proc. Natl. Acad. Sci. USA *116*, 17970–17979. https://doi.org/10.1073/pnas.1906512116.

Newman, A.M., Liu, C.L., Green, M.R., Gentles, A.J., Feng, W., Xu, Y., Hoang, C.D., Diehn, M., and Alizadeh, A.A. (2015). Robust enumeration of cell subsets from tissue expression profiles. Nat. Methods *12*, 453–457. https://doi.org/10.1038/nmeth.3337.

Oikonomou, E.K., and Antoniades, C. (2019). The role of adipose tissue in cardiovascular health and disease. Nat. Rev. Cardiol. *16*, 83–99. https://doi.org/10.1038/s41569-018-0097-6.

Pimpalwar, N., Czuba, T., Smith, M.L., Nilsson, J., Gidlöf, O., and Smith, J.G. (2020). Methods for isolation and transcriptional profiling of individual cells from the human heart. Heliyon *6*, e05810. https://doi.org/10.1016/j.heliyon.2020.e05810.

Pontén, F., Jirström, K., and Uhlen, M. (2008). The human protein atlas - a tool for pathology. J. Pathol. *216*, 387–393. https://doi.org/10.1002/path.2440.

Raajendiran, A., Ooi, G., Bayliss, J., O'Brien, P.E., Schittenhelm, R.B., Clark, A.K., Taylor, R.A., Rodeheffer, M.S., Burton, P.R., and Watt, M.J. (2019). Identification of metabolically distinct adipocyte progenitor cells in human adipose tissues. Cell Rep. *27*, 1528–1540.e7. https://doi.org/10.1016/j.celrep.2019.04.010.

Ritter, A., Friemel, A., Kreis, N.N., Hoock, S.C., Roth, S., Kielland-Kaisen, U., Brüggmann, D., Solbach, C., Louwen, F., and Yuan, J. (2018). Primary cilia are dysfunctional in obese adipose-derived mesenchymal stem cells. Stem Cell Rep. *10*, 583–599. https://doi.org/10.1016/j.stemcr.2017.12.022.

Rizzetto, S., Eltahla, A.A., Lin, P., Bull, R., Lloyd, A.R., Ho, J.W.K., Venturi, V., and Luciani, F. (2017). Impact of sequencing depth and read length on single cell RNA sequencing data of T cells. Sci. Rep. Uk *7*, 12781. https://doi.org/10.1038/s41598-017-12989-x.

Roh, H.C., Tsai, L.T.Y., Lyubetskaya, A., Tenen, D., Kumari, M., and Rosen, E.D. (2017). Simultaneous transcriptional and epigenomic profiling from specific cell types within heterogeneous tissues *in vivo*. Cell Rep. *18*, 1048–1061. https://doi.org/10.1016/j.celrep.2016.12.087.

Rondini, E.A., and Granneman, J.G. (2020). Single cell approaches to address adipose tissue stromal cell heterogeneity. Biochem. J. *477*, 583–600. https://doi.org/10.1042/bcj20190467.

Rotondo, F., Ho-Palma, A.C., Remesar, X., Fernández-López, J.A., Romero, M.D.M., and Alemany, M. (2017). Glycerol is synthesized and secreted by adipocytes to dispose of excess glucose, via glycerogenesis and increased acyl-glycerol turnover. Sci. Rep. *7*, 8983. https://doi.org/10.1038/s41598-017-09450-4.

Rouillard, A.D., Gundersen, G.W., Fernandez, N.F., Wang, Z., Monteiro, C.D., McDermott, M.G., and Ma'ayan, A. (2016). The Harmonizome: A Collection of Processed Datasets Gathered to Serve and Mine Knowledge about Genes and Proteins (Database).

Sadkowski, T., Ciecierska, A., Majewska, A., Oprządek, J., Dasiewicz, K., Ollik, M., Wicik, Z., and Motyl, T. (2014). Transcriptional background of beef marbling - novel genes implicated in intramuscular fat deposition. Meat Sci. *97*, 32–41. https://doi.org/10.1016/j.meatsci.2013.12.017.

Sakurai, T. (2012). The role of NrCAM in neural development and disorders–beyond a simple glue in the brain. Mol. Cell. Neurosci. *49*, 351–363. https://doi.org/10.1016/j.mcn.2011.12.002.

Saliba, A.-E., Westermann, A.J., Gorski, S.A., and Vogel, J. (2014). Single-cell RNA-seq: advances and future challenges. Nucleic Acids Res. *42*, 8845–8860. https://doi.org/10.1093/nar/gku555.

Schleinitz, D., Krause, K., Wohland, T., Gebhardt, C., Linder, N., Stumvoll, M., Blüher, M., Bechmann, I., Kovacs, P., Gericke, M., and Tönjes, A. (2020). Identification of distinct transcriptome signatures of human adipose tissue from fifteen depots. Eur. J. Hum. Genet. *28*, 1714–1725. https://doi.org/10.1038/s41431-020-0681-1.

Sichien, D., Lambrecht, B.N., Guilliams, M., and Scott, C.L. (2017). Development of conventional dendritic cells: from common bone marrow progenitors to multiple subsets in peripheral tissues. Mucosal Immunol. *10*, 831–844. https://doi.org/10.1038/mi.2017.8.

Singh, R.K., Singh, D., Yadava, A., and Srivastava, A.K. (2020). Molecular fossils "pseudogenes" as functional signature in biological system. Genes Genomics *42*, 619–630. https://doi.org/10.1007/s13258-020-00935-7.

Squillaro, T., Peluso, G., Galderisi, U., and Di Bernardo, G. (2020). Long non-coding RNAs in regulation of adipogenesis and adipose tissue function. Elife *9*, e59053. https://doi.org/10.7554/elife.59053.

Statello, L., Guo, C.J., Chen, L.L., and Huarte, M. (2021). Gene regulation by long non-coding RNAs and its biological functions. Nat. Rev. Mol. Cell Biol., 96–118. https://doi.org/10.1038/s41580-020-00315-9.

Stuczyńska, A., Piórkowska, K., Tyra, M., and Zukowski, K. (2018). The effect of QTL-rich region polymorphisms identified by targeted DNA-seq on pig production traits. Mol. Biol. Rep. *45*, 361–371. https://doi.org/10.1007/s11033-018-4170-3.

Sun, T., Fu, M., Bookout, A.L., Kliewer, S.A., and Mangelsdorf, D.J. (2009). MicroRNA let-7 regulates 3T3-L1 adipogenesis. Mol. Endocrinol. *23*, 925–931. https://doi.org/10.1210/me.2008-0298.

Sun, W., Dong, H., Balaz, M., Slyper, M., Drokhlyansky, E., Colleluori, G., Giordano, A., Kovanicova, Z., Stefanicka, P., Balazova, L., et al. (2020). snRNA-seq

reveals a subpopulation of adipocytes that regulates thermogenesis. Nature *587*, 98–102. https://doi.org/10.1038/s41586-020-2856-x.

Sun, W., von Meyenn, F., Peleg-Raibstein, D., and Wolfrum, C. (2019). Environmental and nutritional effects regulating adipose tissue function and metabolism across generations. Adv. Sci. *6*, 1900275. https://doi.org/10.1002/advs.201900275.

Svoboda, M., Portois, L., and Malaisse, W.J. (1999). Glucose regulation of the expression of the glucagon receptor gene. Mol. Genet. Metab. *68*, 258–267. https://doi.org/10.1006/mgme.1999.2913.

Tabula Muris Consortium; Overall coordination; Logistical coordination; Organ collection and processing; Library preparation and sequencing; Computational data analysis; Cell type annotation; Writing group; Supplemental text writing group; Principal investigators (2018). Single-cell transcriptomics of 20 mouse organs creates a Tabula Muris. Nature *562*, 367–372. https://doi.org/10.1038/s41586-018-0590-4.

Tabula Sapiens Consortium; Jones, R.C., Karkanias, J., Krasnow, M.A., Pisco, A.O., Quake, S.R., Salzman, J., Yosef, N., Bulthaup, B., Brown, P., Hemenez, M., et al. (2022). The Tabula Sapiens: a multiple-organ, single-cell transcriptomic atlas of humans. Science *376*, eabl4896. https://doi.org/10.1126/science.abl4896.

Takeda, A., Hollmén, M., Dermadi, D., Pan, J., Brulois, K.F., Kaukonen, R., Lönnberg, T., Boström, P., Koskivuo, I., Irjala, H., et al. (2019). Single-cell survey of human lymphatics unveils marked endothelial cell heterogeneity and mechanisms of homing for neutrophils. Immunity *51*, 561–572.e5. https://doi.org/10.1016/j.immuni.2019.06.027.

Thrupp, N., Sala Frigerio, C., Wolfs, L., Skene, N.G., Fattorelli, N., Poovathingal, S., Fourne, Y., Matthews, P.M., Theys, T., Mancuso, R., et al. (2020). Single-nucleus RNA-seq is not suitable for detection of microglial activation genes in humans. Cell Rep. *32*, 108189. https://doi.org/10.1016/j.celrep.2020.108189.

Uhlen, M., Fagerberg, L., Hallstrom, B.M., Lindskog, C., Oksvold, P., Mardinoglu, A., Sivertsson, A., Kampf, C., Sjostedt, E., Asplund, A., et al. (2015). Proteomics. Tissue-based map of the human proteome. Science *347*, 1260419. https://doi.org/10.1126/science.1260419.

Uhlen, M., Karlsson, M.J., Zhong, W., Tebani, A., Pou, C., Mikes, J., Lakshmikanth, T., Forsström, B., Edfors, F., Odeberg, J., et al. (2019). A genome-wide transcriptomic analysis of protein-coding genes in human blood cells. Science *366*, eaax9198. https://doi.org/10.1126/science.aax9198.

Uhlen, M., Zhang, C., Lee, S., Sjöstedt, E., Fagerberg, L., Bidkhori, G., Benfeitas, R., Arif, M., Liu, Z., Edfors, F., et al. (2017). A pathology atlas of the human cancer transcriptome. Science *357*, eaan2507. https://doi.org/10.1126/science.aan2507.

Valencak, T.G., Osterrieder, A., and Schulz, T.J. (2017). Sex matters: the effects of biological sex on adipose tissue biology and energy metabolism. Redox Biol. *12*, 806–813. https://doi.org/10.1016/j.redox.2017.04.012.

Vijay, J., Gauthier, M.F., Biswell, R.L., Louiselle, D.A., Johnston, J.J., Cheung, W.A., Belden, B., Pramatarova, A., Biertho, L., Gibson, M., et al. (2020). Single-cell analysis of human adipose tissue identifies depot and disease specific cell types. Nat. Metab. *2*, 97–109. https://doi.org/10.1038/s42255-019-0152-6.

Viswanadha, S., and Londos, C. (2006). Optimized conditions for measuring lipolysis in murine primary adipocytes. J. Lipid Res. *47*, 1859–1864. https://doi.org/10.1194/jlr.d600005-jlr200.

Walley, A.J., Jacobson, P., Falchi, M., Bottolo, L., Andersson, J.C., Petretto, E., Bonnefond, A., Vaillant, E., Lecoeur, C., Vatin, V., et al. (2012). Differential coexpression analysis of obesity-associated networks in human subcutaneous adipose tissue. Int. J. Obes. *36*, 137–147. https://doi.org/10.1038/ijo.2011.22.

Wang, G., Zhang, X., Lee, J.S., Wang, X., Yang, Z.Q., and Zhang, K. (2012). Endoplasmic reticulum factor ERLIN2 regulates cytosolic lipid content in cancer cells. Biochem. J. *446*, 415–425. https://doi.org/10.1042/bj20112050.

Wang, S., Pisco, A.O., McGeever, A., Brbic, M., Zitnik, M., Darmanis, S., Leskovec, J., Karkanias, J., and Altman, R.B. (2021). Leveraging the Cell Ontology to classify unseen cell types. Nat. Commun. *12*, 5556. https://doi.org/10.1038/s41467-021-25725-x.

Wu, X., Niculite, C.M., Preda, M.B., Rossi, A., Tebaldi, T., Butoi, E., White, M.K., Tudoran, O.M., Petrusca, D.N., Jannasch, A.S., et al. (2020). Regulation of cellular sterol homeostasis by the oxygen responsive noncoding RNA lincNORS. Nat. Commun. *11*, 4755. https://doi.org/10.1038/s41467-020-18411-x.

Xu, D., and Sun, L. (2020). A functional non-conserved long non-coding RNA in human adipose tissue. Nat. Metab. *2*, 385–386. https://doi.org/10.1038/s42255-020-0208-7.

Yang, H., Qu, H., Huang, H., Mu, Z., Mao, M., Xie, Q., Wang, K., and Hu, B. (2021). Exosomes-mediated transfer of long noncoding RNA LINC01133 represses bladder cancer progression via regulating the Wnt signaling pathway. Cell Biol. Int. *45*, 1510–1522. https://doi.org/10.1002/cbin.11590.

Zhang, X., Lan, Y., Xu, J., Quan, F., Zhao, E., Deng, C., Luo, T., Xu, L., Liao, G., Yan, M., et al. (2019). CellMarker: a manually curated resource of cell markers in human and mouse. Nucleic Acids Res. *47*, D721–D728. https://doi.org/10.1093/nar/gky900.

Ziegenhain, C., Vieth, B., Parekh, S., Reinius, B., Guillaumet-Adkins, A., Smets, M., Leonhardt, H., Heyn, H., Hellmann, I., and Enard, W. (2017). Comparative analysis of single-cell RNA sequencing methods. Mol. Cell *65*, 631–643.e4. https://doi.org/10.1016/j.molcel.2017.01.023.

STAR★METHODS

KEY RESOURCES TABLE

REAGENT or RESOURCE	SOURCE	IDENTIFIER
Antibodies		
Anti-ACSL1 polyclonal antibody produced in rabbit	Human Protein Atlas (www.proteinatlas.org)/ Atlas Antibodies (www.atlasantibodies.com)	Cat#HPA011316; RRID:AB_1844536
Anti-ACO1 polyclonal antibody produced in rabbit	Human Protein Atlas (www.proteinatlas.org)/ Atlas Antibodies (www.atlasantibodies.com)	Cat#HPA019371; RRID:AB_1844519
Anti-FBXO27 polyclonal antibody produced in rabbit	Human Protein Atlas (www.proteinatlas.org)/ Atlas Antibodies (www.atlasantibodies.com)	Cat#HPA046800; RRID:AB_2679813
Anti-MYH9 polyclonal antibody produced in rabbit	Human Protein Atlas (www.proteinatlas.org)/ Atlas Antibodies (www.atlasantibodies.com)	Cat#HPA064783; RRID:AB_2732721
Anti-GIMAP4 polyclonal antibody produced in rabbit	Human Protein Atlas (www.proteinatlas.org)/ Atlas Antibodies (www.atlasantibodies.com)	Cat#HPA019135; RRID:AB_1849670
Anti-FLNB polyclonal antibody produced in rabbit	Human Protein Atlas (www.proteinatlas.org)/ Atlas Antibodies (www.atlasantibodies.com)	Cat#HPA004886; RRID:AB_1848600
Anti-PLN polyclonal antibody produced in rabbit	Human Protein Atlas (www.proteinatlas.org)/ Atlas Antibodies (www.atlasantibodies.com)	Cat#HPA026900; RRID:AB_1855314
Anti-LMOD1 polyclonal antibody produced in rabbit	Human Protein Atlas (www.proteinatlas.org)/ Atlas Antibodies (www.atlasantibodies.com)	Cat#HPA028435; RRID:AB_10602180
Anti-DES polyclonal antibody produced in rabbit	Human Protein Atlas (www.proteinatlas.org)/ Atlas Antibodies (www.atlasantibodies.com)	Cat#HPA018803; RRID:AB_1847616
Anti-TBXAS1 polyclonal antibody produced in rabbit	Human Protein Atlas (www.proteinatlas.org)/ Atlas Antibodies (www.atlasantibodies.com)	Cat#HPA031257; RRID:AB_2673812
Anti-ITGB2 polyclonal antibody produced in rabbit	Human Protein Atlas (www.proteinatlas.org)/ Atlas Antibodies (www.atlasantibodies.com)	Cat#HPA016894; RRID:AB_1846257
Anti-NKG2D (KLRK1) monoclonal antibody produced in mouse	Merck (www.merckmillipore.com)	Cat#05-945; Clone 3.1.1.1 (HPA:CAB021896)
Anti-TYROBP polyclonal antibody produced in rabbit	Santa Cruz Biotechnology (www.scbt.com)	Cat#sc-20783; RRID:AB_638987 (HPA:CAB009493)
Anti- TBX21 polyclonal antibody produced in rabbit	Santa Cruz Biotechnology (www.scbt.com)	Cat#sc-21003; RRID:AB_2200557 (HPA:CAB009524)
Anti- ZAP70 monoclonal antibody produced in mouse	Thermo Fisher Scientific (www.thermofisher.com)	Cat#MS-1911 Clone: 2F3.2 (HPA:CAB002625)
Anti-PRKAR2B polyclonal antibody produced in rabbit	Human Protein Atlas (www.proteinatlas.org)/ Atlas Antibodies (www.atlasantibodies.com)	Cat#HPA008421, RRID:AB_1855421
Anti-C19orf12 polyclonal antibody produced in rabbit	Human Protein Atlas (www.proteinatlas.org)/ Atlas Antibodies (www.atlasantibodies.com)	Cat#HPA046930, RRID:AB_10962836
Anti-CDH13 monoclonal antibody produced in rat	R&D Systems (www.rndsystems.com)	Cat#MAB3264 Clone: 392411 (HPA:CAB025863)
Anti-SHANK3 polyclonal antibody produced in rabbit	Human Protein Atlas (www.proteinatlas.org)/ Atlas Antibodies (www.atlasantibodies.com)	Cat#HPA003446; RRID:AB_1079958
Anti-CASQ2 polyclonal antibody produced in rabbit	Human Protein Atlas (www.proteinatlas.org)/ Atlas Antibodies (www.atlasantibodies.com)	Cat#HPA027285; RRID:AB_1845933
Anti-SLC30A3 polyclonal antibody produced in rabbit	Human Protein Atlas (www.proteinatlas.org)/ Atlas Antibodies (www.atlasantibodies.com)	Cat#HPA060505; RRID:AB_2684296
Anti-IFI30 polyclonal antibody produced in rabbit	Human Protein Atlas (www.proteinatlas.org)/ Atlas Antibodies (www.atlasantibodies.com)	Cat#HPA026650; RRID:AB_10602237

(*Continued on next page*)

Continued

REAGENT or RESOURCE	SOURCE	IDENTIFIER
Anti-LCP1 polyclonal antibody produced in rabbit	Human Protein Atlas (www.proteinatlas.org)/ Atlas Antibodies (www.atlasantibodies.com)	Cat#HPA019493; RRID:AB_1855457
Anti-SP140 polyclonal antibody produced in rabbit	Human Protein Atlas (www.proteinatlas.org)/ Atlas Antibodies (www.atlasantibodies.com)	Cat#HPA006162; RRID:AB_1857403
Anti-CD247 polyclonal antibody produced in rabbit	Human Protein Atlas (www.proteinatlas.org)/ Atlas Antibodies (www.atlasantibodies.com)	Cat#HPA008750; RRID:AB_1857863
Biological samples		
Adipose tissue samples	Uppsala biobank Uhelen et al. (2015) Proteomics. Tissue-based map of the human proteome . Science *347*, 1260419.	https://www.proteinatlas.org/
Deposited data		
All generated data (also contained in manuscript Tables S1, S2, and S3)	This paper	Butler, Lynn (2022), "A human adipose tissue cell type transcriptome atlas", Mendeley Data, V1, https://doi.org/10.17632/6wmbw2nt4x.1
Software and algorithms		
R	R Core Team (2022). R: A language and environment for statistical computing.	https://www.R-project.org
RStudio	RStudio Team (2021). RStudio: Integrated Development Environment for R.	http://www.rstudio.com/
Code for cell type enrichment analysis	This paper	https://github.com/PhilipDusart/cell-enrichment
WCGNA clustering analysis	Langfelder and Horvath, (2008) WGCNA: an R package for weighted correlation network analysis. BMC Bioinformatics *9*, 559	https://horvath.genetics.ucla.edu/html/CoexpressionNetwork/Rpackages/WGCNA/
Seurat single cell RNAseq analysis	Hao et al., (2021). Integrated analysis of multimodal single-cell data. Cell *184*, 3573-3587 e3529	https://satijalab.org/seurat/
Circlize package, for creation of circular plots	Gu et al., (2014) Circlize Implements and enhances circular visualization in R. Bioinformatics *30*, 2811-2812.	https://jokergoo.github.io/circlize_book/book/
GraphPad Prism 6	GraphPad	www.graphpad.com/
Other		
Adipose-visceral (omentum) RNAseq data Adipose-subcutaneous RNAseq data	Genotype-Tissue Expression (GTEx) Project	gtexportal.org; dbGaP Accession phs000424.v8.p2
GO Biological process and Reactome pathways analysis	Ashburner et al. (2000) Gene ontology: tool for the unification of biology. Nat Genet. May 25(1):25-9. The Gene Ontology resource: enriching a GOld mine. (2021) Nucleic Acids Res. 49(D1):D325-D334.	Gene ontology resource and PANTHER classification resource; http://geneontology.org/ GO Ontology database https://doi.org/10.5281/zenodo.4081749 Released 2020-10-09 Reactome version 65. Released 2020-11-17
scRNAseq human subcutaneous adipose tissue	Hildreth et al. (2021). Single-cell sequencing of human white adipose tissue identifies new cell states in health and obesity. Nat Immunol *22*, 639-653.	https://www.nature.com/articles/s41590-021-00922-4 (https://doi.org/10.1038/s41590-021-00922-4;) PMID: **33907320**
scRNAseq human subcutaneous adipose tissue	Sapiens, T. (2021). The Tabula Sapiens: a multiple organ single cell transcriptomic atlas of humans. bioRxiv preprint	https://www.biorxiv.org/content/10.1101/2021.07.19.452956v3 (https://doi.org/10.1101/2021.07.19.452956)

(*Continued on next page*)

Continued

REAGENT or RESOURCE	SOURCE	IDENTIFIER
scRNA murine adipose tissue data	Tabula Muris et al. (2018). Single-cell transcriptomics of 20 mouse organs creates a Tabula Muris. Nature *562*, 367-372.	https://www.nature.com/articles/s41586-018-0590-4 (https://doi.org/10.1038/s41586-018-0590-4) PMID: **30283141**
snRNAseq human subcutaneous adipose tissue	Sun et al. (2020). snRNA-seq reveals a subpopulation of adipocytes that regulates thermogenesis. Nature *587*, 98-102.	https://www.nature.com/articles/s41586-020-2856-x (https://doi.org/10.1038/s41586-020-2856-x) PMID: **33116305**
Website resource for protein coding gene enrichment	This paper	Human Protein Atlas https://www.proteinatlas.org/humanproteome/tissue+cell+type/adipose+tissue
Website resource for non-protein coding gene enrichment	This paper	https://cell-enrichment.shinyapps.io/noncoding/

RESOURCE AVAILABILITY

Lead contact

Further information and requests for resources and reagents should be directed to and will be fulfilled by the Lead Contact: Dr. Lynn Marie Butler. Email: Lynn.butler@ki.se.

Materials availability

This study did not generate new unique reagents.

Data and code availability

- This paper analyses existing, publicly available data. The accession number for the datasets are listed in the key resources table.
- All original code has been deposited at GitHub and is publicly available as of the date of publication. DOIs are listed in the key resources table.
- Any additional information required to reanalyze the data reported in this paper is available from the lead contact upon request.

EXPERIMENTAL MODEL AND SUBJECT DETAILS

Bulk RNA-seq data analyzed in this study was obtained from the Genotype-Tissue Expression (GTEx) Project (gtexportal.org) (Consortium, 2015) accessed on 2019.11.29 (dbGaP Accession phs000424.v8.p2). Sample IDs of visceral adipose tissue (VAT) and subcutaneous adipose tissue (SAT) samples used in the analysis can be found in Table S1. Human tissue protein profiling was performed in house as part of the Human Protein Atlas (HPA) project (Ponten et al., 2008; Uhlen et al., 2015, 2017) (www.proteinatlas.org). Adipose tissue samples were obtained from the Department of Pathology, Uppsala University Hospital, Uppsala, Sweden, as part of the Uppsala Biobank. Samples were handled in accordance with Swedish laws and regulations, with approval from the Uppsala Ethical Review Board (Uhlen et al., 2015).

METHOD DETAILS

Tissue profiling: human tissue sections

Adipose tissue sections were stained, as previously described (Ponten et al., 2008; Uhlen et al., 2015). Briefly, formalin fixed and paraffin embedded tissue samples were sectioned, de-paraffinized in xylene, hydrated in graded alcohols and blocked for endogenous peroxidase in 0.3% hydrogen peroxide diluted in 95% ethanol. For antigen retrieval, a Decloaking chamber® (Biocare Medical, CA) was used. Slides were boiled in Citrate buffer®, pH6 (Lab Vision, CA). Primary antibodies and a dextran polymer visualization system (UltraVision LP HRP polymer®, Lab Vision) were incubated for 30 min each at room temperature and slides were developed for 10 min using Diaminobenzidine (Lab Vision) as the chromogen. Slides were counterstained in Mayers hematoxylin (Histolab) and scanned using Scanscope XT (Aperio). Primary antibodies, source, target and identifier are as follows: Atlas Antibodies: ACSL1 (Cat#HPA011316; RRID:AB_1844536), ACO1 (Cat#HPA019371; RRID:AB_1844519), FBXO27 (Cat#HPA046800; RRID:AB_2679813), MYH9 (Cat#HPA064783; RRID:AB_2732721), GIMAP4 (Cat#HPA019135; RRID:AB_1849670), FLNB

(Cat#HPA004886; RRID:AB_1848600), PLN (Cat#HPA026900; RRID:AB_1855314), LMOD1 (Cat#HPA028435; RRID:AB_10602180), DES (Cat#HPA018803; RRID:AB_1847616), TBXAS1 (Cat#HPA031257; RRID:AB_2673812), ITGB2 (Cat#HPA016894; RRID:AB_1846257), PRKAR2B (Cat#HPA008421, RRID:AB_1855421), C19orf12 (Cat#HPA046930, RRID:AB_10962836), SHANK3 (Cat#HPA003446; RRID:AB_1079958), CASQ2 (Cat#HPA027285; RRID:AB_1845933), SLC30A3 (Cat#HPA060505; RRID:AB_2684296), LCP1 (Cat#HPA019493; RRID:AB_1855457), IFI30 (Cat#HPA026650; RRID:AB_10602237), SP140 (Cat#HPA006162; RRID:AB_1857403), CD247 (Cat#HPA008750; RRID:AB_1857863). Santa Cruz: TYROBP (Cat#sc-20783; RRID:AB_638987), TBX21 (Cat#sc-21003; RRID:AB_2200557), Thermo Fisher Scientific: ZAP70 (Cat#MS-1911), Merck: KLRK1 (Cat#05-945;), R&D Systems: CDH13 (Cat#MAB3264). All IHC images are available on the HPA website (https://www.proteinatlas.org/).

QUANTIFICATION AND STATISTICAL ANALYSIS

Reference transcript-based correlation analysis

This method was adapted and expanded from that previously developed to determine the cross-tissue pan-EC-enriched transcriptome (Butler et al., 2016) and human brain cell enriched genes (Dusart et al., 2019). Pairwise Spearman correlation coefficients were calculated between reference transcripts selected as proxy markers for: adipocytes [*ADIPOQ*, *LIPE*, *PLIN1*], adipocyte progenitor cells [*FKBP10*, *COL6A1*, *COL6A2*], mesothelial cells [*UPK3B*, *MSLN*, *KRT19*], endothelial cells [*MMRN2*, *ESAM*, *CDH5*], smooth muscle cells [*KCNMB1*, *CNN1*, *MYH11*], macrophages [*CD68*, *C1QC*, *FCER1G*], neutrophils [*CSF3R*, *FCGR3B*, *CXCR2*], mast cells [*CPA3*, *TPSB2*, *TPSAB1*], T cells [*TRBC2*, *CD6*, *CD3E*] and plasma cells [*IGKC*, *JCHAIN*, *MZB1*] and all other sequenced transcripts. Transcripts with a TPM value < 0.1 in more than 50% of samples were excluded from analysis (but are still included in data tables). See results section for full criteria required for transcript classification of transcripts as cell-type enriched (also Table S1, tab 1, table B). Correlation coefficients were calculated in R using the *corr.test* function from the *psych* package (v 1.8.4). In addition to correlation coefficients False Discovery Rate (FDR) adjusted p-values (using Bonferroni correction) and raw p-values were calculated. FDR <0.0001 for correlation was required for inclusion as cell type enriched, but no transcripts in either VAT or SAT required exclusion due to this criterion.

Weighted correlation network (WGCNA) analysis

The R package WGCNA (Langfelder and Horvath, 2008) was used to perform co-expression network analysis for gene clustering, on log2 expression TPM values. The analysis was performed according to recommendations in the WGCNA manual. Transcripts with too many missing values were excluded using the goodSamplesGenes() function. The remaining genes were used to cluster the samples, and obvious outlier samples were excluded.

Gene ontology and reactome analysis

The Gene Ontology Consortium (Ashburner et al., 2000) and PANTHER classification resource (Mi et al., 2013, 2016) were used to identify over represented terms (biological processes) in the panel of identified cell-type-enriched transcripts from the GO ontology (release date 2021-10-09) or reactome (release date 2021-11-17) databases.

Processing of data from adipose tissue scRNA-seq and snRNA-seq datasets

Data from scRNA-seq analysis of human SAT (Hildreth et al., 2021; Tabula Sapiens et al., 2022), scRNA-seq of murine adipose tissue (mixed depot) (Tabula Muris et al., 2018) and snRNA-seq of human SAT (Sun et al., 2020) was downloaded or received from the authors upon request. Cell type clustering and categorization was performed as originally described, but immune cell subtypes in (Hildreth et al., 2021) were merged, and myofibroblasts and smooth muscle cells in (Tabula Sapiens et al., 2022) were handled together. The R Seurat package (Hao et al., 2021) and the FindAllMarkers function was used to determine the Log2 fold change values for each gene in all cell types versus all others within each study, and to generate illustrative UMAP plots when required. The statistical significance of overlap between cell-type enriched genes in each study was calculated using a hypergeometric test (Figure S5). Criteria used for comparison of our cell type-enriched datasets with expression profiles in the independent studies are given in the relevant results sections and associated tables or figure legends.

Visualization

Circular graphs (Figures 3, 4B, and 6E) were constructed using the R package *circlize* (Gu et al., 2014). Some figure sections were created with BioRender.com.

ADDITIONAL RESOURCES

Analyzed data for all protein coding genes is provided on the Human Protein Atlas website: (www.proteinatlas.org/humanproteome/tissue+cell+type/adipose+tissue). Analyzed data for non-coding transcripts is provided on: https://cell-enrichment.shinyapps.io/noncoding/. The published article includes all datasets generated during this study, including depot- and sex-subset analysis (Tables S1, S2, and S3).

Cell Reports, Volume *40*

Supplemental information

A human adipose tissue cell-type transcriptome atlas

Marthe Norreen-Thorsen, Eike Christopher Struck, Sofia Öling, Martin Zwahlen, Kalle Von Feilitzen, Jacob Odeberg, Cecilia Lindskog, Fredrik Pontén, Mathias Uhlén, Philip James Dusart, and Lynn Marie Butler

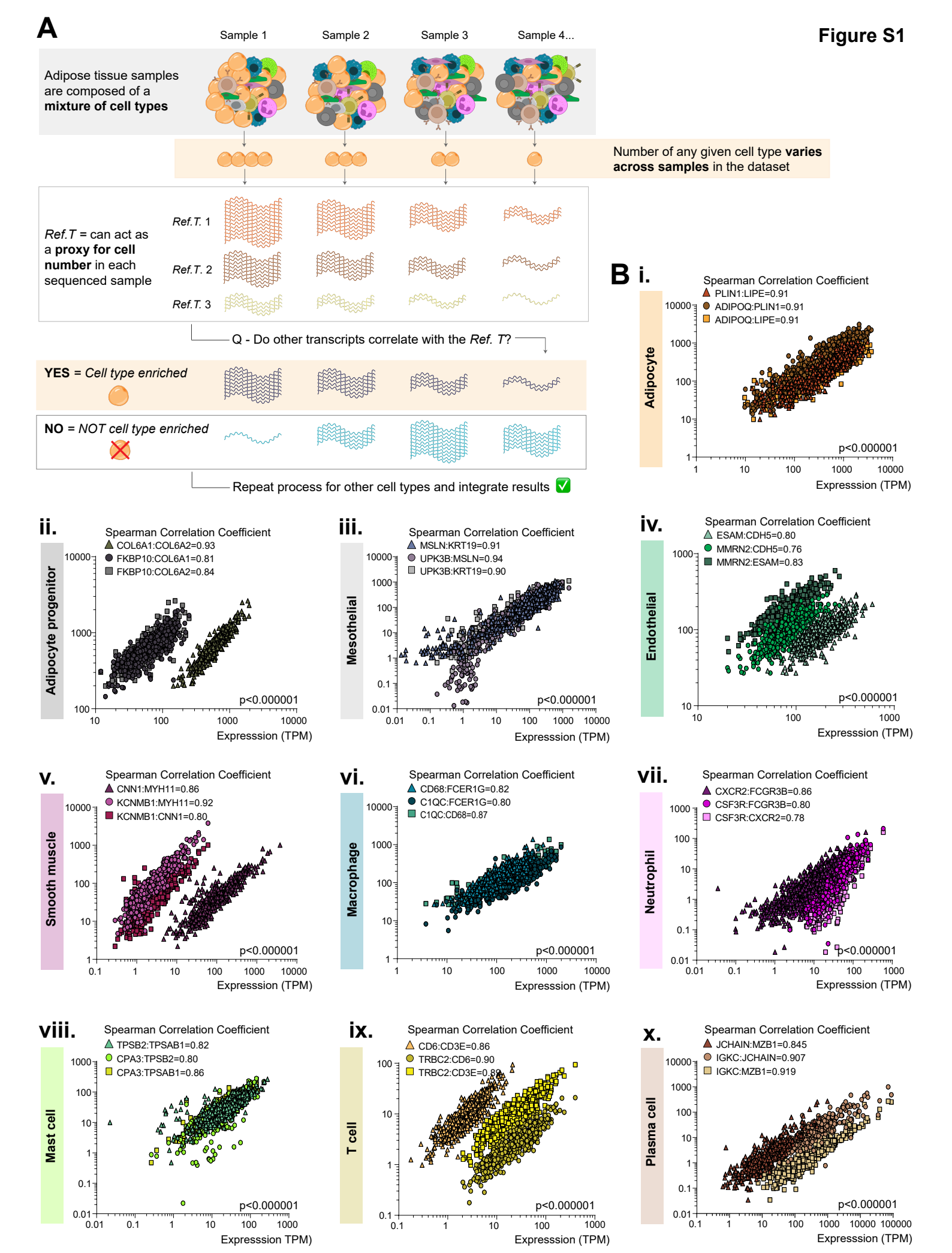
A
Figure S1
Sample 1
Sample 2
Sample 3
Sample 4...
Adipose tissue samples are composed of a **mixture of cell types**
Number of any given cell type **varies across samples** in the dataset
Ref.T = can act as a **proxy for cell number** in each sequenced sample
Ref.T. 1
Ref.T. 2
Ref.T. 3
Q - Do other transcripts correlate with the *Ref. T*?
YES = *Cell type enriched*
NO = *NOT cell type enriched*
Repeat process for other cell types and integrate results
B i.
Adipocyte
Spearman Correlation Coefficient
PLIN1:LIPE=0.91
ADIPOQ:PLIN1=0.91
ADIPOQ:LIPE=0.91
p<0.000001
Expresssion (TPM)
ii.
Adipocyte progenitor
Spearman Correlation Coefficient
COL6A1:COL6A2=0.93
FKBP10:COL6A1=0.81
FKBP10:COL6A2=0.84
p<0.000001
Expresssion (TPM)
iii.
Mesothelial
Spearman Correlation Coefficient
MSLN:KRT19=0.91
UPK3B:MSLN=0.94
UPK3B:KRT19=0.90
p<0.000001
Expresssion (TPM)
iv.
Endothelial
Spearman Correlation Coefficient
ESAM:CDH5=0.80
MMRN2:CDH5=0.76
MMRN2:ESAM=0.83
p<0.000001
Expresssion (TPM)
v.
Smooth muscle
Spearman Correlation Coefficient
CNN1:MYH11=0.86
KCNMB1:MYH11=0.92
KCNMB1:CNN1=0.80
p<0.000001
Expresssion (TPM)
vi.
Macrophage
Spearman Correlation Coefficient
CD68:FCER1G=0.82
C1QC:FCER1G=0.80
C1QC:CD68=0.87
p<0.000001
Expresssion (TPM)
vii.
Neutrophil
Spearman Correlation Coefficient
CXCR2:FCGR3B=0.86
CSF3R:FCGR3B=0.80
CSF3R:CXCR2=0.78
p<0.000001
Expresssion (TPM)
viii.
Mast cell
Spearman Correlation Coefficient
TPSB2:TPSAB1=0.82
CPA3:TPSB2=0.80
CPA3:TPSAB1=0.86
p<0.000001
Expresssion TPM)
ix.
T cell
Spearman Correlation Coefficient
CD6:CD3E=0.86
TRBC2:CD6=0.90
TRBC2:CD3E=0.88
p<0.000001
Expresssion (TPM)
x.
Plasma cell
Spearman Correlation Coefficient
JCHAIN:MZB1=0.845
IGKC:JCHAIN=0.907
IGKC:MZB1=0.919
p<0.000001
Expresssion (TPM)

Figure S1. Methodological summary and expression distribution and correlations between human visceral adipose tissue (VAT) cell type reference transcripts. Related to Figure 1 and Table S1, Tab 1. (**A**) Schematic of analysis concept. (**B**) Expression of *Ref.T* selected to represent: (**i**) adipocytes, (**ii**) adipocyte progenitors, (**iii**) mesothelial cells, (**iv**) endothelial cells, (**v**) smooth muscle cells, (**vi**) macrophages, (**vii**) neutrophils, (**viii**) mast cells, (**ix**) T-cells and (**x**) plasma cells.

Figure S2

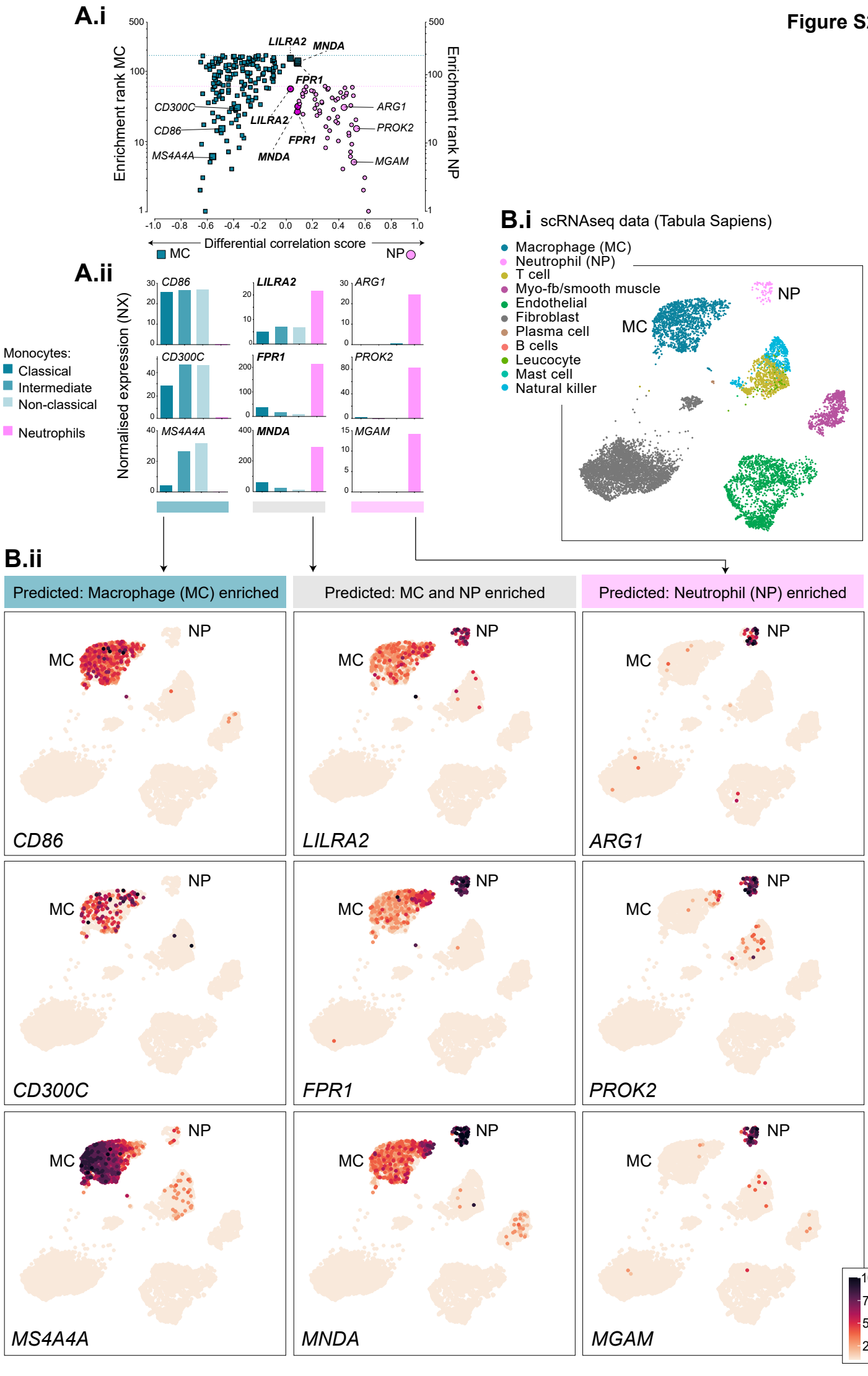
A.i
Enrichment rank MC
Enrichment rank NP
LILRA2
MNDA
FPR1
CD300C
ARG1
LILRA2
PROK2
CD86
FPR1
MS4A4A
MNDA
MGAM
Differential correlation score
MC
NP
A.ii
Normalised expression (NX)
CD86
LILRA2
ARG1
CD300C
FPR1
PROK2
MS4A4A
MNDA
MGAM
Monocytes:
Classical
Intermediate
Non-classical
Neutrophils
B.i scRNAseq data (Tabula Sapiens)
Macrophage (MC)
Neutrophil (NP)
T cell
Myo-fb/smooth muscle
Endothelial
Fibroblast
Plasma cell
B cells
Leucocyte
Mast cell
Natural killer
NP
MC
B.ii
Predicted: Macrophage (MC) enriched
Predicted: MC and NP enriched
Predicted: Neutrophil (NP) enriched
CD86
LILRA2
ARG1
CD300C
FPR1
PROK2
MS4A4A
MNDA
MGAM
10.0
7.5
5.0
2.5

Figure S2. scRNAseq of subcutaneous adipose tissue provides supportive evidence for cell type enrichment predictions from integrative co-expression analysis of unfractionated visceral adipose tissue (VAT). Related to Figure 1D. (**A**) (**i**) For transcripts above the designated correlation threshold with the macrophage (squares, MC) or neutrophil (circles, NP) *Ref.T.* panels, the '*differential correlation score'* (difference between mean corr. with MC and NP *Ref.T.*) was plotted vs. 'enrichment ranking'. Bold text annotations show transcripts appearing in *both* MC- and NP lists (circular *and* square symbol, on the same X-axis dimension). (**ii**) scRNAseq data from the Human Protein Blood Atlas (Uhlen et al., 2019) showing gene expression in classical, intermediate, and non-classical monocytes, and neutrophils from whole blood. (**B**) scRNAseq data from analysis of cell types in human subcutaneous adipose tissue was sourced from Tabula Sapiens (Tabula Sapiens., 2021), and used to generate UMAP plots showing (**i**) scRNAseq cell type annotations, and (**ii**) expression profiles of genes we predicted as macrophage (MC)-enriched [*CD86*, *CD300C*, *MS4A4A*] (blue bar), co-enriched in both MC and neutrophils (NP) [*LILRA2*, *FPR1*, *MNDA*] (grey bar) or predominantly NP-enriched [*ARG1*, *PROK2*, *MGAM*] (pink bar).

Figure S3

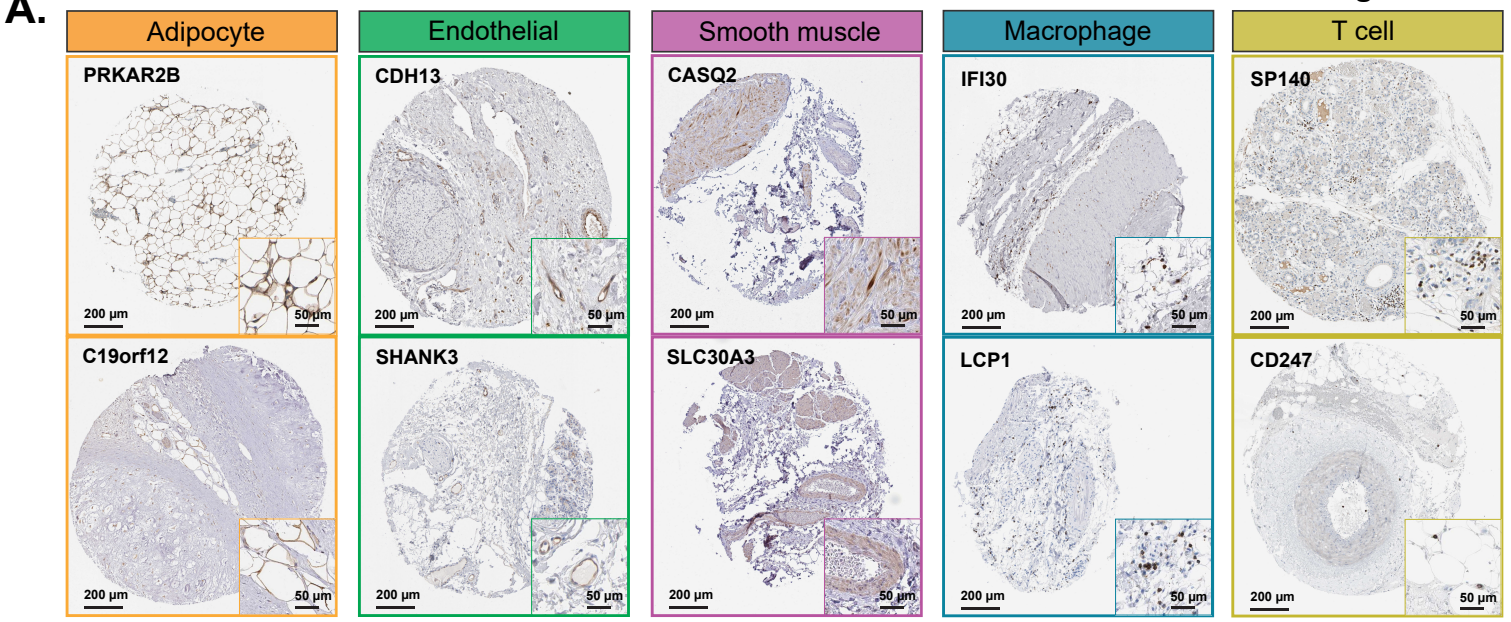
A.
Adipocyte
Endothelial
Smooth muscle
Macrophage
T cell
PRKAR2B
CDH13
CASQ2
IFI30
SP140
C19orf12
SHANK3
SLC30A3
LCP1
CD247
200 µm
50 µm

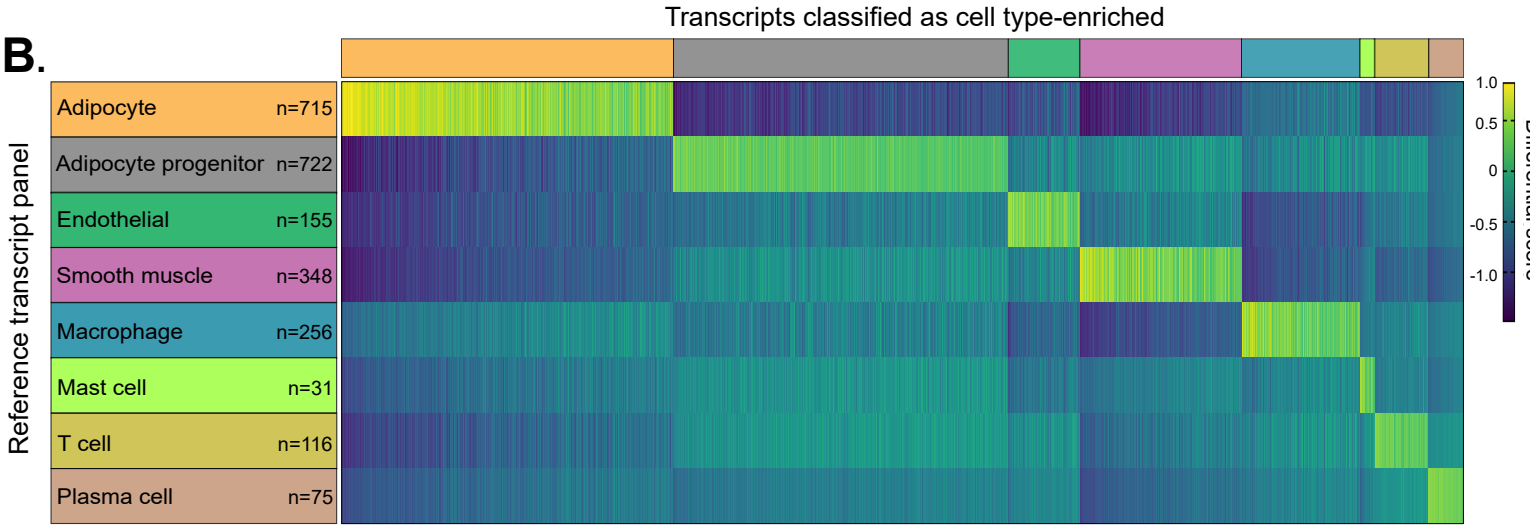
B.
Transcripts classified as cell type-enriched
Reference transcript panel
Adipocyte n=715
Adipocyte progenitor n=722
Endothelial n=155
Smooth muscle n=348
Macrophage n=256
Mast cell n=31
T cell n=116
Plasma cell n=75
Differential score
1.0
0.5
0
-0.5
-1.0

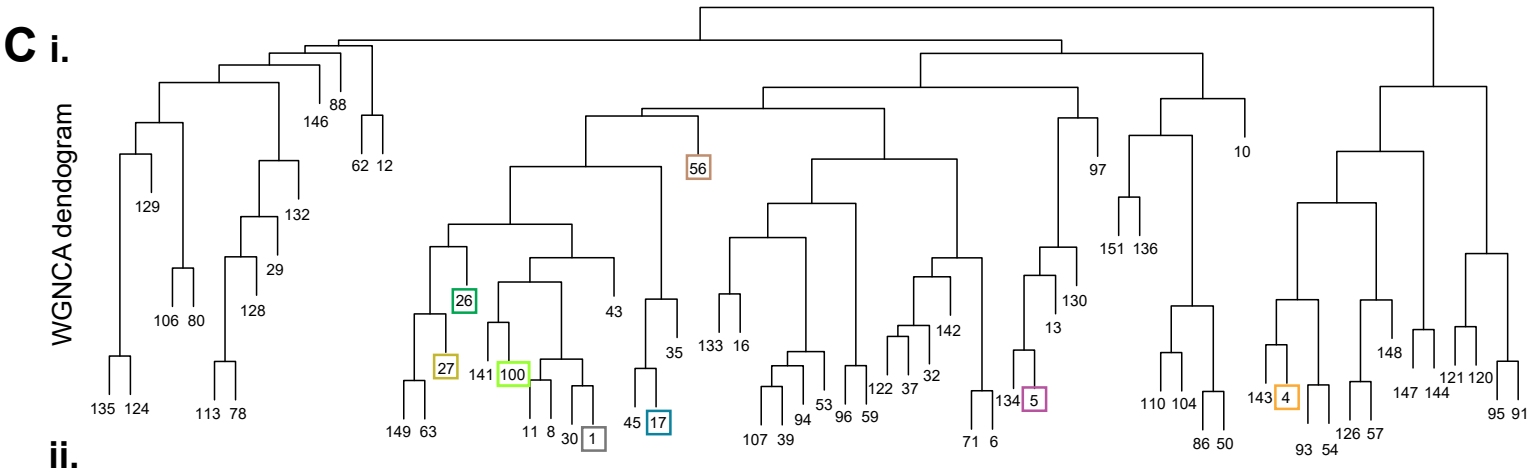
C i.
WGNCA dendogram

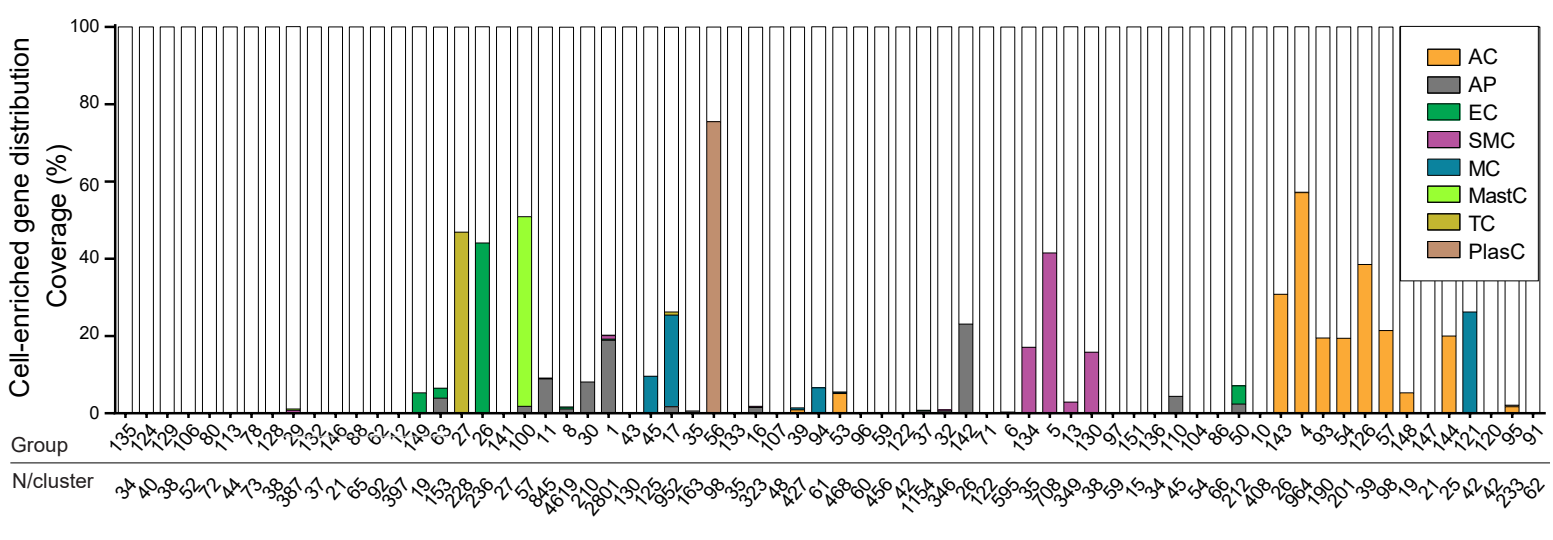
ii.
Cell-enriched gene distribution
Coverage (%)
AC
AP
EC
SMC
MC
MastC
TC
PlasC
Group
N/cluster

Figure S3. (A) Protein profiling of transcripts identified as cell-enriched in VAT. Related to Figure 2. Human adipose tissue sections were stained using primary antibodies targeting proteins encoded by transcripts classified as adipocyte-, endothelial-, smooth muscle-, macrophage- or T-cell-enriched. Scale bar 200μm, inset 50μm. See also Table S2, Tab 1.

(B-C) Integrative co-expression analysis of unfractionated RNAseq reveals enriched transcriptomes of subcutaneous adipose tissue (SAT) cell types. Related to Figure 6, Figure S7, Figure S8. Human SAT RNAseq data (n=646), retrieved from Genotype-Tissue Expression (GTEx) portal V8, was used to determine correlation coefficients (corr.) between selected adipose cell type *Ref.T* and all other sequenced transcripts. (**A**) Heat map plot of transcripts classified as cell type-enriched (indicated by horizontal-coloured bars), showing differential score between mean correlation coefficient with the corresponding *Ref.T.* panel vs. highest mean correlation coefficient amongst the other *Ref.T.* panels. (**B**) SAT RNAseq data was subject to weighted correlation network analysis (WGCNA). (**i**) Coloured squares indicate *Ref.T.* location on resultant dendrogram. (**ii**) Distribution of transcripts classified as cell type-enriched across dendrogram groups. See also Table S2, Tab 1.

Figure S4

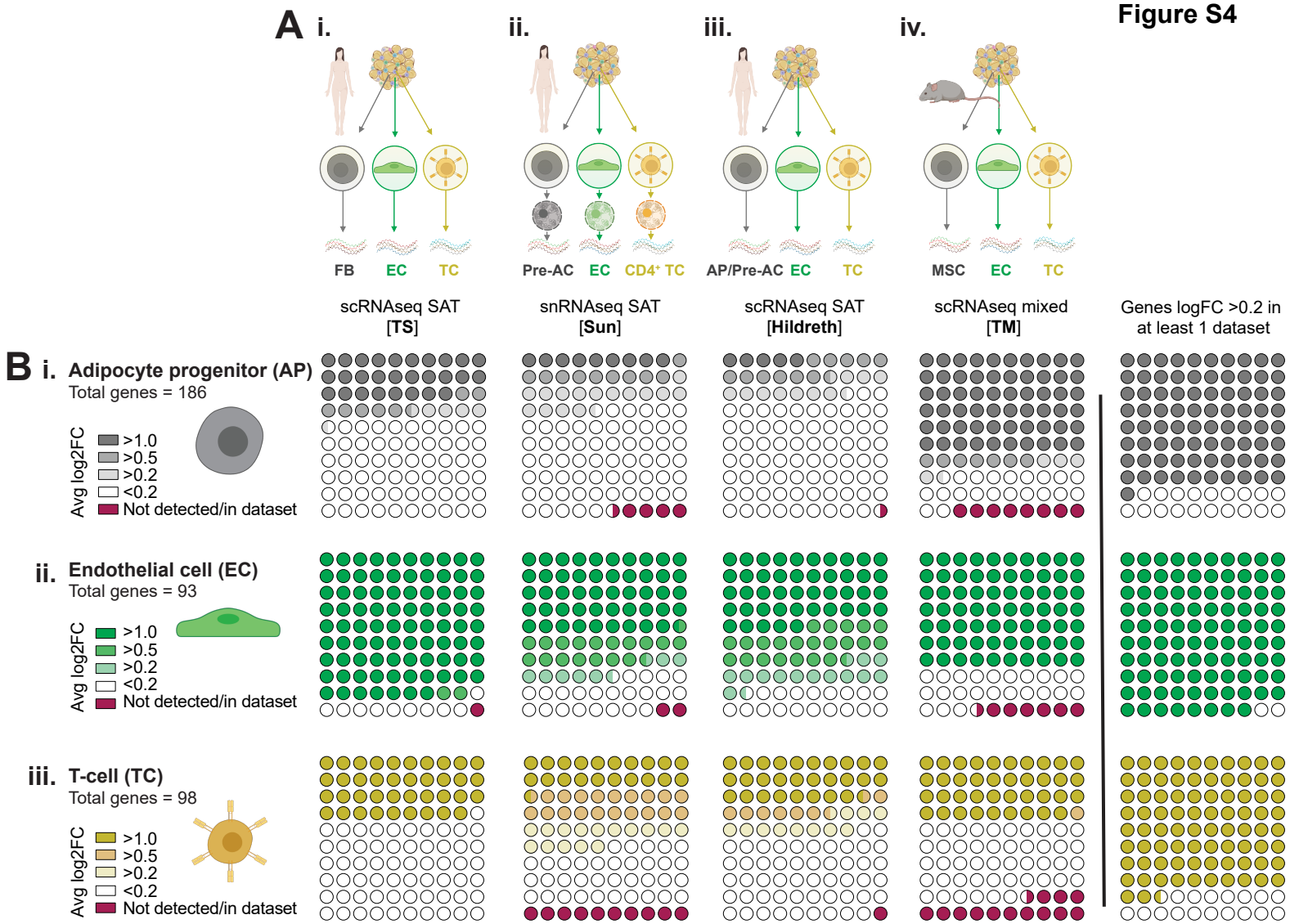
A
i.
ii.
iii.
iv.
FB EC TC
Pre-AC EC CD4+ TC
AP/Pre-AC EC TC
MSC EC TC
scRNAseq SAT [TS]
snRNAseq SAT [Sun]
scRNAseq SAT [Hildreth]
scRNAseq mixed [TM]
Genes logFC >0.2 in at least 1 dataset
B
i. Adipocyte progenitor (AP)
Total genes = 186
ii. Endothelial cell (EC)
Total genes = 93
iii. T-cell (TC)
Total genes = 98
Avg log2FC
>1.0
>0.5
>0.2
<0.2
Not detected/in dataset

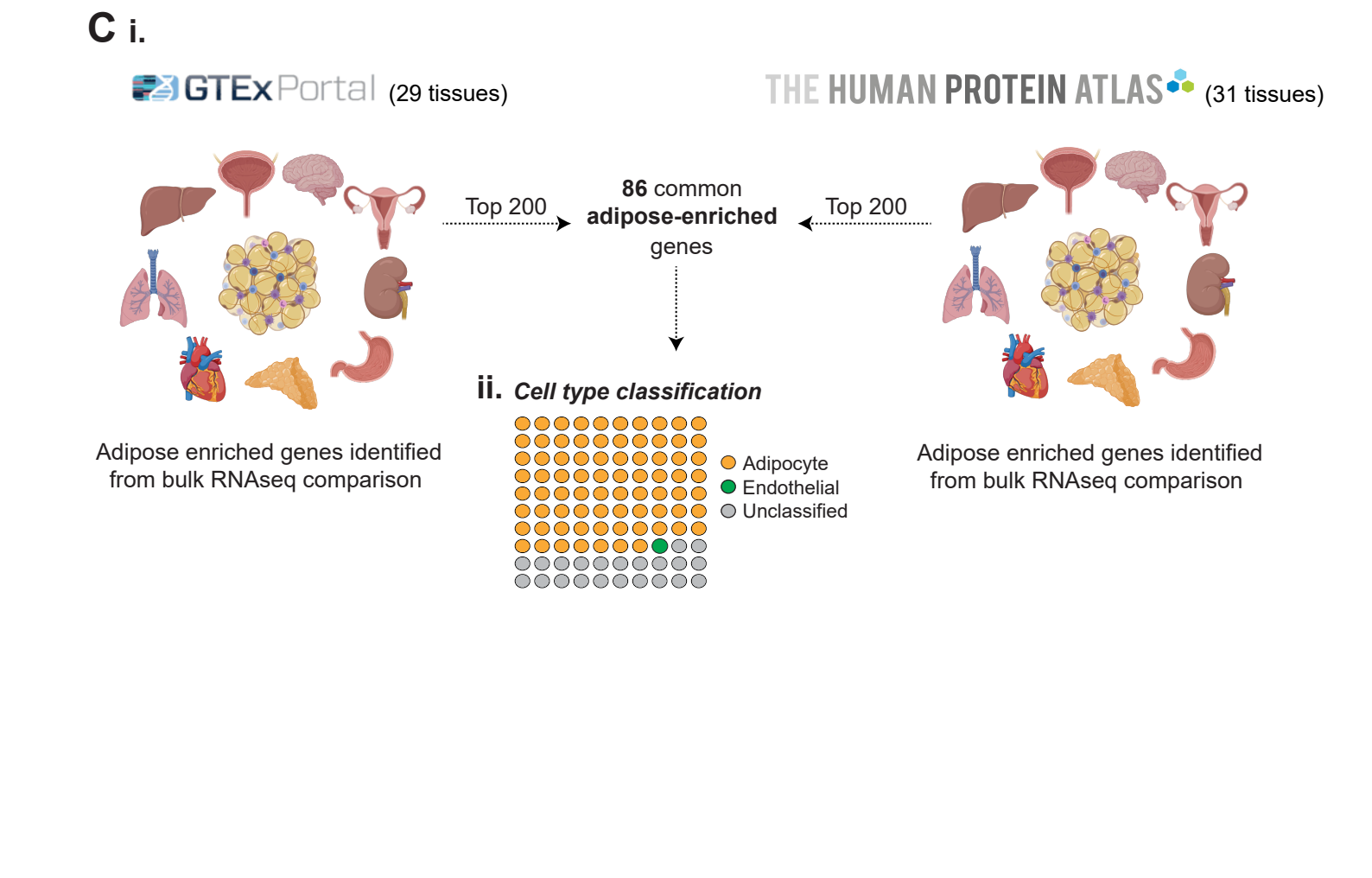
C i.
GTEx Portal (29 tissues)
THE HUMAN PROTEIN ATLAS (31 tissues)
Top 200
86 common adipose-enriched genes
Top 200
Adipose enriched genes identified from bulk RNAseq comparison
Adipose enriched genes identified from bulk RNAseq comparison
ii. Cell type classification
Adipocyte
Endothelial
Unclassified

Figure S4. Comparison of predicted human visceral adipose tissue (VAT) and subcutaneous adipose tissue (SAT) cell type enriched transcriptomes with scRNAseq or snRNAseq of human SAT or murine adipose tissue. Related to Figure 3, Table S1 Tab 5, and Table S2, Tab 1. (**A**) Data generated by single cell (scRNAseq) or single nuclear (snRNAseq) profiling of human SAT or murine adipose tissue was sourced from (**i**) Tabula Sapiens (Tabula Sapiens., 2021) (scRNAseq SAT [TS]), (**ii**) Sun *et al*. (Sun et al., 2020) (snRNAseq SAT [Sun]), (**iii**) Hildreth *et al*. (Hildreth et al., 2021) (ssRNAseq SAT [Hildreth]) and (**iv**) Tabula Muris (Tabula Muris et al., 2018) (scRNAseq mixed [TM]). (**B**) Genes predicted as enriched in (**i**) adipocyte progenitor cells, (**ii**) endothelial cells or (**iii**) T-cells, in both VAT and SAT, were cross checked with the independent studies. Colour coding indicates proportion of genes that have average Log2 fold change >1.0, >0.5 or >0.2 [$p<0.01$] in the corresponding cell type vs. all other cell types profiled in the independent study. **FB**: fibroblast, **AP**: adipocyte progenitor, **Pre-AC**: pre-adipocyte, **MSC**: mesenchymal stem cell, **EC**: endothelial cell, **TC**: T-cell. (**C.i**) The top 200 human adipose enriched genes in Human Protein Atlas and GTEx datasets were sourced from Harminozome database (Rouillard et al., 2016) and (**C.ii**) classification as cell type-enriched in our analysis of VAT determined.

Figure S5

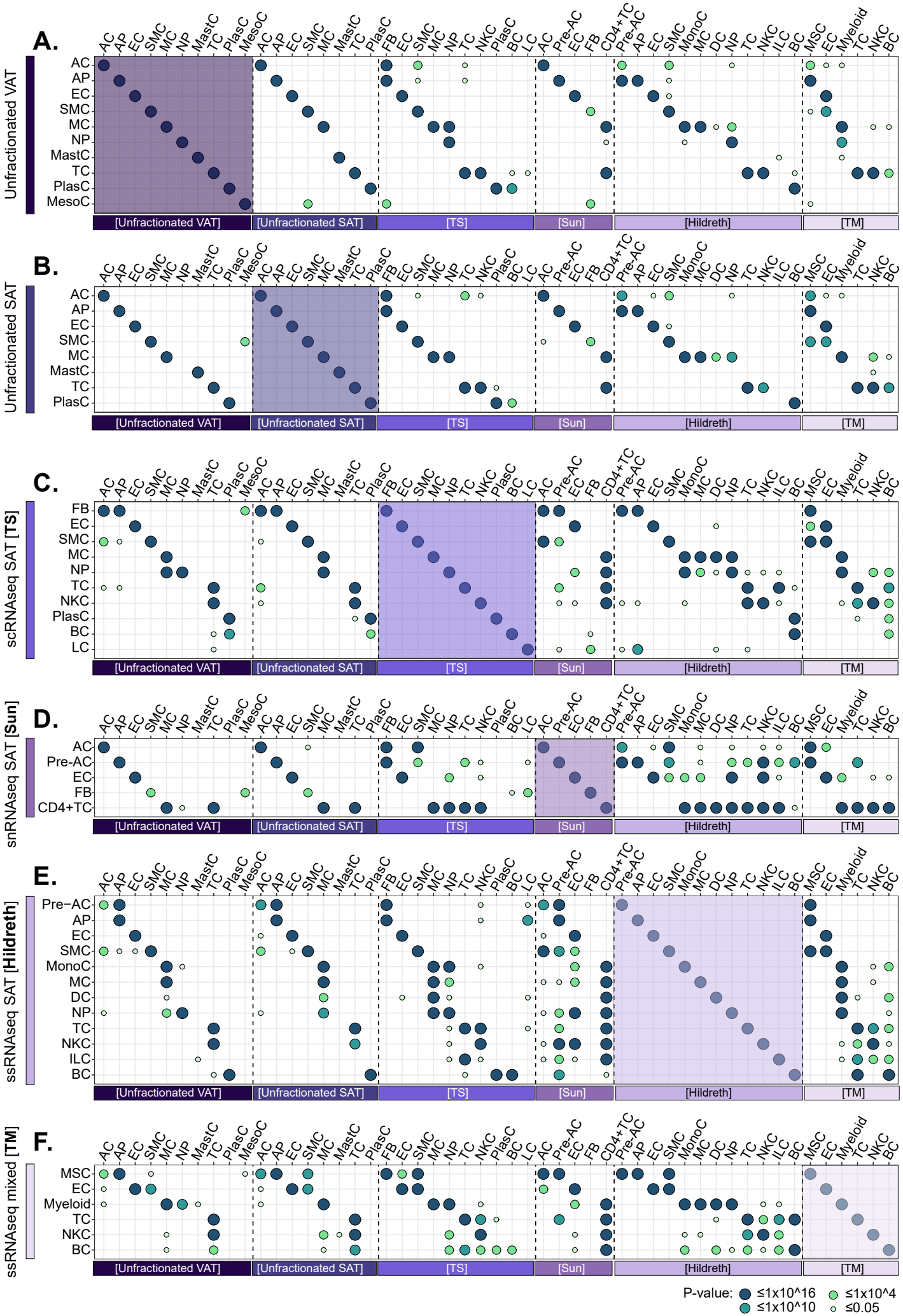
A.
Unfractionated VAT
AC
AP
EC
SMC
MC
NP
MastC
TC
PlasC
MesoC
B.
Unfractionated SAT
C.
scRNAseq SAT [TS]
FB
NKC
BC
LC
D.
snRNAseq SAT [Sun]
Pre-AC
CD4+TC
E.
ssRNAseq SAT [Hildreth]
MonoC
DC
ILC
F.
ssRNAseq mixed [TM]
MSC
Myeloid
[Unfractionated VAT]
[Unfractionated SAT]
[TS]
[Sun]
[Hildreth]
[TM]
P-value:
≤1x10^16
≤1x10^10
≤1x10^4
≤0.05

Figure S5. A comparison of cell-type enriched genes identified in different adipose tissue cell type profiling studies; Related to Figure 3 and S4. Bubble heatmap showing the significance (indicated by dot size and colour) of shared enriched genes between adipose tissue cell types, as identified in the current study using integrative correlation analysis of bulk RNAseq of (**A**) human visceral adipose tissue [VAT] (Unfractionated VAT) and (**B**) human subcutaneous adipose tissue [SAT] (Unfractionated SAT), or by single cell/single nuclear profiling of human SAT, sourced from (**C**) Tabula Sapiens (Tabula Sapiens., 2021) (scRNAseq SAT [TS]) (**D**) Sun *et al*. (Sun et al., 2020) (snRNAseq SAT [Sun]) and (**E**) Hildreth et al. (Hildreth et al., 2021) (ssRNAseq SAT [Hildreth]), or in (**F**) murine adipose tissue from Tabula Muris (Tabula Muris et al., 2018) (scRNAseq mixed [TM]) (enriched genes defined as those ≥0.5 Log2 fold change in expression vs. all other cell types in the same study [$p<0.01$]). Cell type-enriched genes were compared across all studies (indicated by different coloured blocks on x-axis), N.B. not all cell types were represented in every study. When overlap of enriched genes was not statistically significant (hypergeometric test, $P > 0.05$), no dot is displayed. **AC**: adipocyte, **AP**: adipocyte progenitor, **EC**: endothelial cell, **SMC**: smooth muscle cell, **MC**: macrophage, **NP**: neutrophil, **MastC**: mast cell, **TC**: T-cell, **PlasC**: plasma cell, **MesoC**: mesothelial cell, **FB**: fibroblast, **NKC**: natural killer cell, **BC**: B-cell, **LC**: leukocyte, **Pre-AC**: pre-adipocyte, **MonoC**: monocyte, **DC**: dendritic cell, **ILC**: innate lymphoid cell, **MSC**: mesenchymal stem cell.

Figure S6

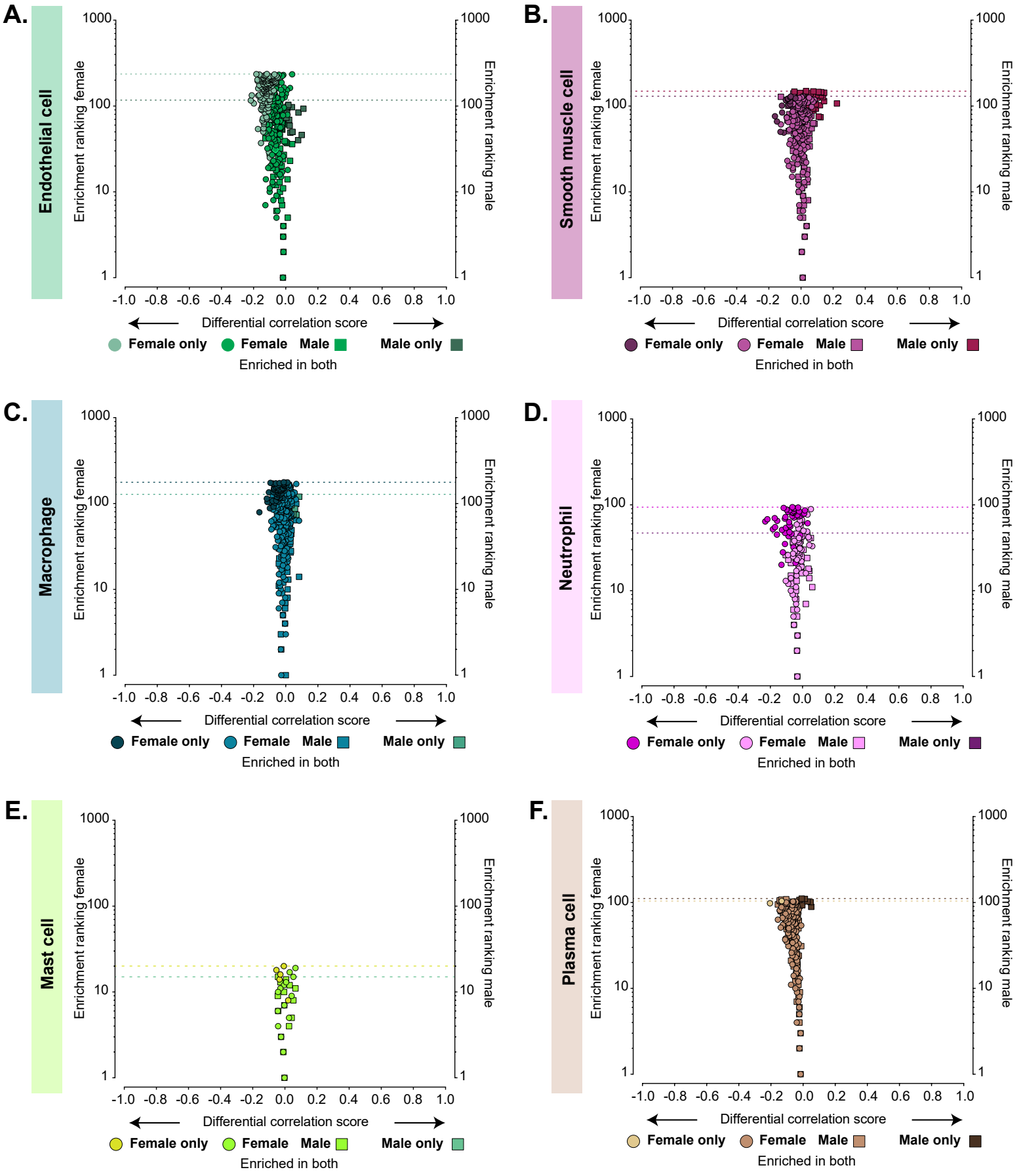
A.
Endothelial cell
B.
Smooth muscle cell
C.
Macrophage
D.
Neutrophil
E.
Mast cell
F.
Plasma cell
Enrichment ranking female
Enrichment ranking male
1000
100
10
1
-1.0 -0.8 -0.6 -0.4 -0.2 0.0 0.2 0.4 0.6 0.8 1.0
Differential correlation score
Female only
Female
Male
Male only
Enriched in both

Figure S6. Identification of sex-specific cell type-enriched transcripts in human visceral adipose tissue (VAT); Related to Figure 5. VAT RNAseq data (n=527), retrieved from Genotype-Tissue Expression (GTEx) portal V8, was divided into female and male sample subgroups (female n=165, male n=362) before classification of cell type-enriched transcripts (see results section for criteria). For transcripts classified as: (**A**) endothelial, (**B**) smooth muscle, (**C**) macrophage, (**D**) neutrophil, (**E**) mast cell, or (**F**) plasma cell enriched, in either female or male subsets, the *´sex differential correlation score'* (difference between mean corr. with the *Ref.T* panel in females vs. males) was plotted vs. 'enrichment ranking' (position in each respective enriched list, highest corr. = rank 1). On each plot, transcripts classified as enriched in *both* females and males are represented by common coloured circle and square symbols, respectively, and transcripts classified as enriched *only* in females or males are represented by differently coloured circle or square symbols, respectively. Correspondingly coloured threshold lines denote ranking below which transcripts were classified as female or male enriched. See also Table S3, Tab 2.

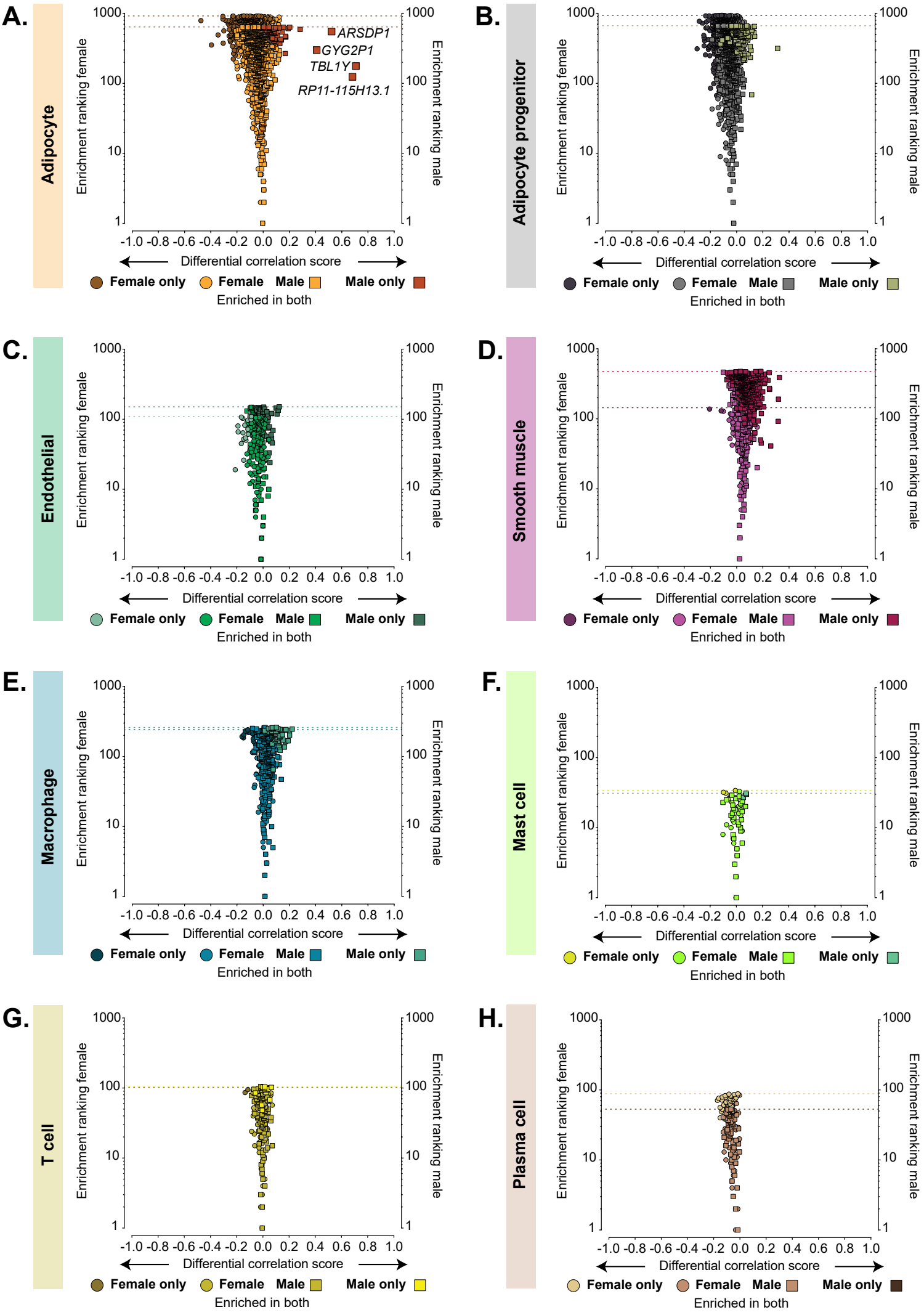
A.
Adipocyte
ARSDP1
GYG2P1
TBL1Y
RP11-115H13.1
B.
Adipocyte progenitor
C.
Endothelial
D.
Smooth muscle
E.
Macrophage
F.
Mast cell
G.
T cell
H.
Plasma cell
Enrichment ranking female
Enrichment ranking male
1000
100
10
1
-1.0 -0.8 -0.6 -0.4 -0.2 0.0 0.2 0.4 0.6 0.8 1.0
Differential correlation score
Female only
Female
Male
Male only
Enriched in both

Figure S7. Identification of sex-specific cell-enriched transcripts in human subcutaneous adipose tissue (SAT); Related to Figure 5. Human SAT RNAseq data (n=646), retrieved from Genotype-Tissue Expression (GTEx) portal V8, was divided into female and male sample subgroups (female n=212, male n=434) before classification of cell type-enriched transcripts (see results section for criteria). For transcripts classified as: (**A**) adipocyte, (**B**) adipocyte progenitor, (**C**) endothelial, (**D**) smooth muscle, (**E**) macrophage (**F**) mast cell, (**G**) T-cell, or (**H**) plasma cell enriched, in either female or male subsets, the *´sex differential correlation score'* (difference between mean corr. with the *Ref.T* panel in females vs. males) was plotted vs. 'enrichment ranking' (position in each respective enriched list, highest corr. = rank 1). On each plot, transcripts enriched in *both* females and males are represented by common coloured circle and square symbols, respectively, and transcripts classified as enriched *only* in females or males are represented by differently coloured circle or square symbols, respectively. Correspondingly coloured threshold lines denote ranking below which transcripts were classified as female or male enriched. Transcripts with differential corr. score >0.40 are labelled with identifiers. See also Table S3, Tab 4.

Figure S8

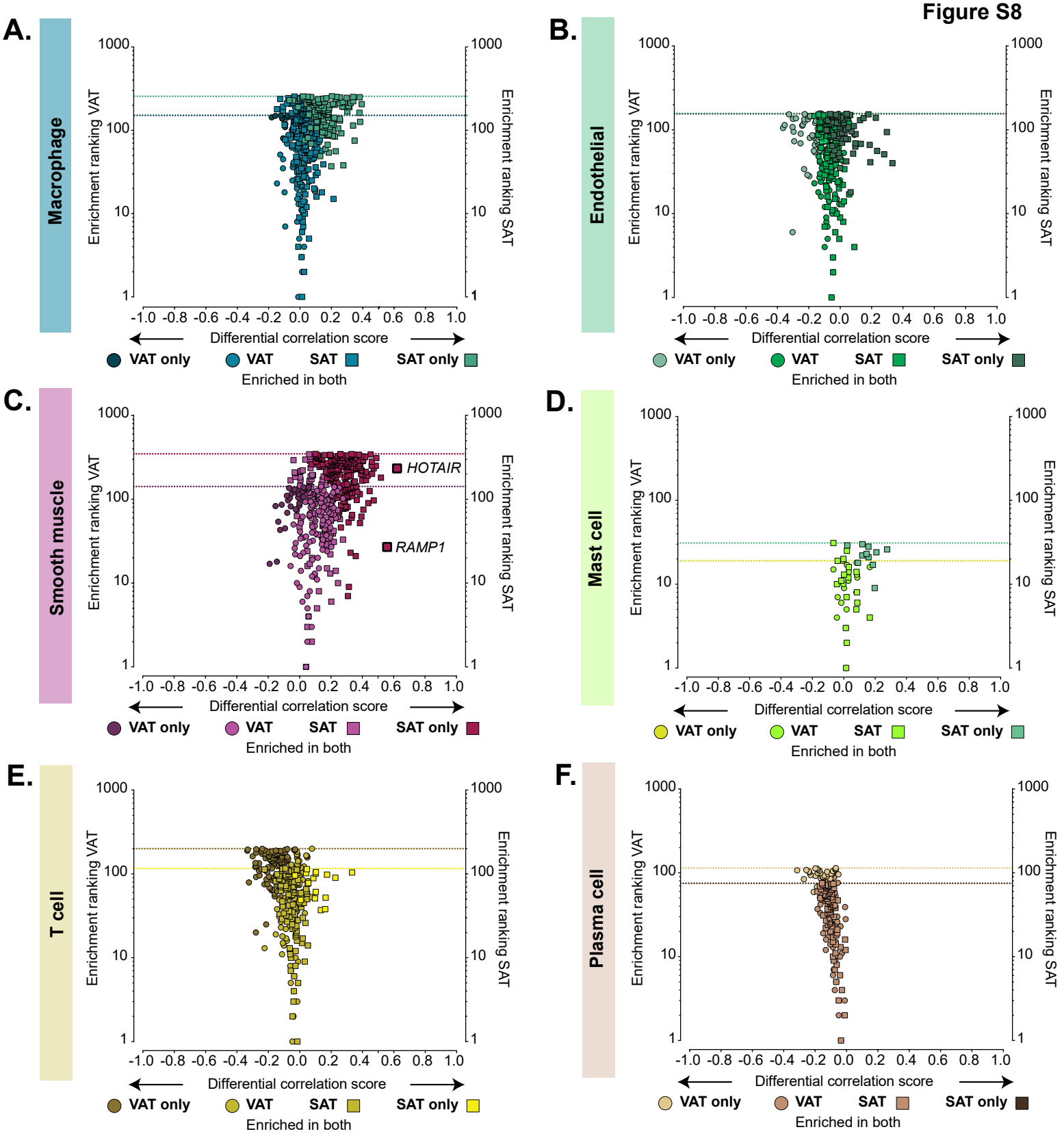
A.
Macrophage
B.
Endothelial
C.
Smooth muscle
HOTAIR
RAMP1
D.
Mast cell
E.
T cell
F.
Plasma cell
Enrichment ranking VAT
Enrichment ranking SAT
1000
100
10
1
-1.0 -0.8 -0.6 -0.4 -0.2 0.0 0.2 0.4 0.6 0.8 1.0
Differential correlation score
VAT only
VAT
SAT
SAT only
Enriched in both

Figure S8. Identification of depot-specific cell-enriched transcripts in human adipose tissue; Related to Figure 6. Human visceral adipose tissue (VAT, n=527) or subcutaneous adipose tissue (SAT, n=646) RNAseq data, retrieved from Genotype-Tissue Expression (GTEx) portal V8, was used for classification of cell type-enriched transcripts (see results section for criteria). For transcripts classified as: (**A**) macrophage, (**B**) endothelial, (**C**) smooth muscle, (**D**) mast cell, (**E**) T-cell, or (**F**) plasma cell enriched, in either VAT or SAT, the *´depot differential correlation score'* (difference between mean corr. with the *Ref.T* panel in VAT vs. SAT) was plotted vs. 'enrichment ranking' (position in each respective enriched list, highest corr. = rank 1). On each plot, transcripts enriched in *both* VAT and SAT are represented by common coloured circle and square symbols, respectively, and transcripts classified as enriched *only* in VAT or SAT are represented by differently coloured circle or square symbols, respectively. Correspondingly coloured threshold lines denote ranking below which transcripts were classified as VAT or SAT enriched. Selected transcripts with differential corr. score >0.40 are labelled with identifiers.